Air–Sea Interactions and Biogeochemical Responses to Medicane Daniel

Babita Jangir and Ehud Strobach
Institute of Soil, Water and Environmental Sciences, Volcani Institute, Agriculture Research Organization, Rishon LeTsiyon, Israel
*Corresponding author: Babita Jangir (bj11@iitbbs.ac.in)

Abstract: Medicane Daniel, formed on 4-12 September 2023, ~~has stood~~stands out as the deadliest recorded storm in Mediterranean history. In this study, we investigate the role of sea features ~~as contributors to~~in the intensification of the ~~Medicane~~medicane Daniel~~.~~ and the response of biogeochemical properties to the storm. Our ~~findings reveal the presence~~results show that medicane Daniel intensified immediately prior to landfall in a coastal environment characterized by the co-occurrence of a warm-~~-~~core eddy (WCE), ~~high~~elevated ocean heat content, and a moderate marine ~~heat wave (MHW) at the location where Medicane Daniel intensified. These features were situated near the coastal region, facilitating~~heatwave, highlighting the ~~Medicane's~~role of pre-existing upper-ocean thermal conditions in supporting its intensification ~~close to the coast. Consequently, the Medicane did not weaken significantly after landfall, leading to severe damage along the coast of Libya. These conditions favoured the Medicane's intensification and, due to high moisture convergence, contributed to significant precipitation at the eddy and MHW position. Importantly~~. Additionally, observations from the high-resolution Surface Water and Ocean Topography (SWOT) satellite ~~captured the WCE more accurately or in finer detail. This allowed for attribution of changes in biogeochemical properties—namely, chlorophyll, phytoplankton, nutrients, and dissolved oxygen concentrations due to eddy-induced~~ reveal a larger anticyclonic eddy than that depicted in lower-resolution products, thereby further supporting the hypothesis of sea-induced intensification. The favorable conditions before landfall enhanced moisture convergence and moisture supply, leading to intense precipitation in this region. Biogeochemical properties were strongly affected by cyclone-induced subsurface vertical mixing and upwelling. ~~The biogeochemical properties tend to increase over the WCE and MHW locations due to mixing and upwelling induced by the presence of the WCE and MHW. Our case-study analysis suggests that, under atmospheric cyclone conditions, subsurface mixing may be more influential within CCEs than upwelling driven by Ekman pumping, which, by contrast, may play a more prominent role within WCEs~~Focusing on two eddies in the vicinity of the

maximum cyclone intensity, we found that the observed vertical displacement of the deep chlorophyll maximum exceeds that expected by direct wind-driven upwelling alone, suggesting additional contribution from a structural isopycnal adjustment triggered by the neutralization of eddy vorticity. We propose that the medicane destabilize the eddies' internal balance, leading to a large-scale reorganization of the water column that persists longer in the WCE than the transient response observed in the CCE.

Key Words: Medicanes, eddies, ~~Marine Heat Wave, deadliest Medicane~~marine heatwave, medicane Daniel, SWOT satellite, Biogeochemistry

Key Points:

- ~~Along the path of Medicane Daniel, Warm Core Eddy (WCE), Ocean Heat Content, and Marine Heatwave (MHW) were present near the coastal region. Their combined presence enhanced precipitation, making Medicane Daniel a deadly storm.~~
- ~~SWOT satellite products better represent air-sea interaction due to their fine resolution over eddy regions.~~
- ~~An increase in surface chlorophyll was observed after the cyclone passed over the WCE location. Positive Ekman pumping confirms that the increase was caused by cyclone-induced upwelling.~~

- ~~Analysis of~~Co-occurring warm-core eddies, marine heatwave, and elevated ocean heat content created optimal conditions for the rapid intensification of Medicane Daniel near landfall.

- High-resolution SWOT observations reveal stronger and larger eddy structures than conventional datasets, highlighting their critical role in air–sea interactions.
- Interaction with warm-core eddies amplifies vertical ~~profiles shows a decrease in surface temperature and an increase in chlorophyll and nutrient concentration above the mixed layer due to cyclone-induced~~ mixing and ~~upwelling.~~

- ~~Cross-section analysis over the WCE location shows an upward shift in isotherms~~nutrient supply, leading to ~~increased~~enhanced chlorophyll ~~from cyclone-induced mixing~~ and ~~upwelling.~~ productivity responses.

- Cyclone-induced biogeochemical response is influenced by subsurface restructuring and isopycnal adjustment, exceeding expectations from Ekman-driven upwelling alone.

- Results demonstrate that compound ocean extremes can significantly enhance both cyclone intensity and ocean biogeochemical impacts.

1. Introduction:

The Mediterranean region ~~(MR)~~ is recognized as a climate change hotspot (IPCC, 2021), warming at a rate up to 1.5 times faster than the global average (MedECC, 2020; Zittis et al., 2022; Khodayar et al., 2025). ~~Positioned~~Situated between the arid climate of North Africa and the temperate and wet climate of Central Europe, the ~~MR~~Mediterranean region is particularly vulnerable to future climate impacts. Surface temperature in this region is projected to continue increasing, but the precipitation tends to decrease (Cherif et al., 2020; Reale et al., 2022). As a consequence, the magnitude of extreme ~~phenomena~~events such as Mediterranean cyclones, marine ~~heat waves (MHW~~heatwaves (MHWs), and intense droughts is projected to increase under future climate scenarios (MedECC, 2020; Hochman et al., 2021; Zittis et al., 2022).

Medicanes are a subcategory of Mediterranean cyclones, which can resemble hurricanes in both intensity and impact. They often bring torrential rainfall, flash floods, powerful winds, storm surges, and hazardous sea conditions. Such events pose significant risks, particularly to coastal communities and urban centers, threatening homes, livelihoods, and natural ecosystems (Hochman et al., 2021; Khodayar et al., 2025). Similar to Mediterranean cyclones, ~~their~~medicane's intensity is projected to increase under future climate scenarios, but with lower frequency (González-Alemán et al., 2019). Despite their strong impact, the full extent of the damage medicanes inflict, both socially and economically, remains insufficiently understood. Moreover, their potential impact on ocean biogeochemistry is under-researched and often ~~inadequately~~poorly communicated, leaving a critical gap in public awareness and scientific insight.

Medicanes are also known as 'tropical-like cyclones' because they have tropical cyclone-like characteristics such as a cloud-free calm "eye," ~~spiraling~~spiralling cloud bands, and strong winds near the vortex ~~center~~centre. These features may be associated with the absence of fronts, weak vertical wind shear, and a warm--core ~~(WC)~~ with an axisymmetric structure (Miglietta et

al., 2019; Flaounas et al., 2022; Panegrossi et al., 2023). The formation of cyclones in the ~~MR,~~Mediterranean region including medicanes, is primarily driven by baroclinic instability and Rossby wave breaking (Raveh-Rubin and Flaounas, 2017; Flaounas et al., 2022). As these systems evolve and reach their mature stage, medicanes can intensify and be sustained through exchanges of heat and momentum at the air-sea interface (Emanuel, 2005). The development of intense Mediterranean cyclones is frequently associated with southward shifts of the polar jet, which enable air masses with high potential vorticity ~~(PV)~~ to enter the ~~MR~~Mediterranean region, thereby initiating baroclinic instability similar to that observed during extratropical cyclone development over open oceans (Flocas, 2000; Trigo et al., 2002; Nicolaides et al., 2006; Fita et al., 2007; Claud et al., 2010; Kouroutzoglou et al., 2011; Flaounas et al., 2015). Raveh-Rubin and Flaounas (2017) identified Rossby ~~Wave Breaking (RWB)~~wave breaking as a frequent precursor to Mediterranean cyclogenesis, while Flaounas et al. (2015) further emphasized that the cyclogenesis environment in the region is characterized by strong horizontal shear, driving these cyclones to follow a typical baroclinic life cycle. Furthermore, Flaounas et al. (2025) also highlight the importance of these atmospheric variables in the genesis and intensification of Medicane Daniel. ~~However, in~~In this manuscript, we primarily focus on ~~the Atmospheric~~potential atmospheric and oceanic ~~precursor~~precursors that are ~~most directly~~ associated with Daniel's intensification and ~~associated~~ensuing precipitation.

Furthermore~~,,~~, the role of underlying ocean eddies and ~~MHW~~marine heatwaves in modulating the deepening of a cyclone is often overlooked. Recent studies have highlighted the critical role of ocean eddies and MHWs in modulating cyclone's deepening in the ~~MR~~Mediterranean region (Jangir et al., 2023, 2024; Mishra et al., 2024; Strobach et al., 2024). In particular, Jangir et al. (2024) demonstrated the significant intensification of medicane Ianos due to the presence of a strong MHW, making it the only category 2 cyclone observed in the Mediterranean Sea ~~(MS).~~. In contrast, other medicanes such as Zorbas and Apollo intensified primarily due to the interaction with ~~Warm Core Eddies~~warm-core eddies (WCEs) along their paths. Mishra et al. (2024) reported that if we remove these Sea Surface Temperature (SST) anomalies from the path of medicane Ianos, the medicane will still form, but with a reduced intensity. Strobach et al. (2024) reported that ocean mesoscale eddies in the Eastern Mediterranean can significantly influence extreme weather, as shown during the heavy rainfall event in Israel that occurred from January 8 to 10, 2020. High-resolution coupled ocean-atmosphere simulations captured the event more accurately than uncoupled ones. The study by Strobach et al. (2024) highlights

how eddies can enhance atmospheric moisture and meso-cyclone development, intensifying local extremes.

As efforts continue to enhance the accuracy of cyclone intensity forecasts, the potential influence of eddies ~~MHW~~, marine heatwaves, and ocean heat content (OHC) remains a critical yet less explored aspect, particularly within the Mediterranean context. To improve the prediction of Mediterranean cyclones and mitigate associated risks, a deeper understanding of air-sea interaction processes, specifically surface heat fluxes, momentum fluxes, and upper-ocean thermodynamic responses, and the role of pre-existing oceanic conditions in cyclone genesis and intensification, is essential. Recent studies have increasingly focused on these dynamics, exploring how air-sea exchanges affect not only medicanes intensity but also the ocean's biogeochemical responses (Jangir et al., 2023; Menna et al., 2023; Scardino et al., 2024; Avolio et al., 2024). Notably, Jangir et al. (2023) highlighted the influence of WCEs on the intensification of medicanes, demonstrating that eddy size also plays a critical role; larger eddies tend to promote stronger cyclones and heavier rainfall. In this particular study, we show the influence of eddies and ~~MHW~~marine heatwave on the intensity of medicane Daniel.

Most of the studies use the satellite sea level anomaly (SLA) altimetry data from the Copernicus Marine Services (CMEMS) for the detection of eddies. Here, we also use the Surface Water and Ocean Topography (SWOT) satellite data, which are available at high spatial resolution. The SWOT satellite provides the first-ever global observations of ocean dynamics at sub-mesoscale spatial resolutions (1–100 km). While traditional satellite products, such as those from the Copernicus mission, offer spatial resolutions of approximately 25 km globally and 12.5 km in the ~~MS~~Mediterranean Sea, SWOT's advanced wide-swath altimetry overcomes these limitations by achieving resolutions as fine as 250 m to 2 km. This enhanced capability enables the detection of small-scale ocean features that were previously unresolved. SWOT observations confirm the widespread presence of sub-mesoscale eddies and internal waves, particularly energetic in regions like western boundary currents and the Antarctic Circumpolar Current (Archer et al., 2025; Tranchant et al., 2025). This high-resolution data is especially valuable for studying ocean-atmosphere interactions, such as the role of eddies in cyclone intensification. In particular, SWOT's ability to capture the structure, intensity, and evolution of eddies provides critical insight into how these features influence heat transport, vertical mixing, and the modulation of cyclone intensity due to eddies. Thus, SWOT marks a

transformative step in advancing our understanding of fine-scale ocean processes and their implications for weather, climate, and marine biogeochemistry.

~~Cyclones~~Atmospheric cyclones are known to trigger substantial phytoplankton blooms (Shang et al., 2015; Chowdhury et al., 2020; Liu et al., 2020). These blooms are primarily attributed to cyclone-induced upwelling and vertical mixing, which transport cold, nutrient-rich, or chlorophyll-loaded water into the euphotic zone, stimulating phytoplankton bloom. Such storm-driven biological responses offer valuable insight into ocean mixing and biogeochemical dynamics (Chen et al., 2022). Additionally, strong cyclonic winds often cause a noticeable decrease in SST, which plays a crucial role in regulating primary productivity (Latha et al., 2015). There are a few studies reported in the other ocean basins that indicate the enhancement of chlorophyll- a (Chl-a) concentration following the passage of a cyclone in the presence of eddies (Dutta et al., 2019; Zhang and Qui, 2020; Vidya et al., 2021) and ~~MHW~~marine heatwave (Oliver et al., 2018; Jangir et al., 2024). Recently, a study by Scardino et al. (2025) reported the response of Mediterranean cyclones on ocean chlorophyll concentration, primarily using Bio-Argo floats. In contrast, our study offers a new perspective by utilizing subsurface profiles of a broader suite of biogeochemical variables, including chlorophyll, phytoplankton, nutrients, and oxygen concentration, complemented by multiple ocean satellite and reanalysis products. To date, such a comprehensive assessment has rarely been reported for the Mediterranean Sea. Here, we investigate the impact of ~~Medicane~~medicane Daniel on ocean biogeochemistry in the context of the SST anomalies along its path.

In this study, we highlight the co-occurrence of compound extreme events in the region prior to medicane Daniel's landfall. Specifically, we show that the intensification of medicane Daniel may have been driven by the combined influence of a WCE and ~~an MHW.~~a marine heatwave. We examine the key atmospheric and oceanic factors that contributed to Daniel's development~~, ultimately making it one of the deadliest cyclones in the MS.~~. The analysis also ~~covers the critical role of~~highlights the unique perspective offered by the SWOT satellite ~~in advancing~~, capturing aspects of air-sea interaction ~~research; this is the first study to report the importance of SWOT data for air-sea interaction in the MS.~~that traditional datasets do not resolve. Additionally, we investigate the medicane's impact on ocean biogeochemistry along its path, and specifically at the WCE location prior to landfall, providing insights into the underlying physical and biological processes that govern such interactions.

~~**2. Medicane Daniel Synoptic Overview and Intensification:** Daniel was formed in the MS from 4 to 12 September 2023. It was the deadliest cyclone in the Mediterranean basin during the satellite era. The cyclone originated from an upper-level cut-off low and brought exceptionally heavy rainfall to Greece and Libya, triggering severe floods and mudslides. These catastrophic events led to at least 5,898 fatalities in Libya (Hérincs, 2023; Normand et al., 2024).~~

2. Synoptic evolution and impacts of medicane Daniel: On September 2-3, a swift cold front traversed Central Europe, generating an upper-level trough that created a cut-off low near Greece by September 4. Named "Daniel" by the Hellenic National Weather Service, this cyclone brought severe thunderstorms to Greece, Turkey, and Bulgaria due to unstable atmospheric conditions and warm waters. ~~Moving~~Daniel traversed the Mediterranean Sea from 4 to 12 September 2023, bringing exceptionally heavy rainfall to Greece and Libya and triggering severe floods and mudslides. While moving south-southwest, ~~it~~Daniel stalled over the ~~Central~~central Mediterranean, evolving into a subtropical storm by September 7. By September 9, Daniel transitioned into a tropical-like storm, making landfall in Libya on September 10~~, causing catastrophic floods.~~. Daniel dissipated into a low-pressure trough by September 12 (Hérincs, 2023; Normand et al., 2024). ~~Storm~~Medicane Daniel brought intense winds of up to 120 km/h and delivered a total of 240 mm of rainfall over ~~a~~ 25~~-hour period~~ hours (Normand et al., 2024). It caused catastrophic flash flooding in Derna on September 10, 2023, as torrential rains overwhelmed the river's delta outlet. The flood destroyed large parts of the city's buildings, infrastructure, and bridges, resulting in 8.8 million tons of debris. In Derna alone, 10% of houses were destroyed and 18.5% damaged. In other cities, such as Susah, approximately 28% of homes were destroyed, while Albayda, Al-Marj, and others also suffered heavy losses. Overall, the storm led to 5,898 deaths, 8,000 missing persons, 44,800 displaced individuals, and 18,838 homes damaged across Libya's northeastern coast, making it the deadliest African storm since 1900 (Hérincs, 2023; Normand et al., 2024; Katsanos et al., 2024).

3. Data and Methods:

3.1 Data sources and products used:

In this study, the best-track data for the medicane Daniel was obtained from the Zivipotty Cyclone Report database ~~(https://zivipotty.hu/tcr.html).~~(https://zivipotty.hu/tcr.html). Eddy identification was based on daily SLA fields sourced from the CMEMS. Specifically, the dataset SEALEVEL_EUR_PHY_L4_NRT_OBSERVATIONS_008_060, with a spatial

resolution of 0.125°, was utilized. To detect and characterize the ~~MHW~~marine heatwave, daily SST data from the NOAA Optimum Interpolation SST V2 dataset (Reynolds et al., 2007) were used. This dataset has a spatial resolution of 0.25° and covers the period from 1981 to the present. The key atmospheric variables, including total column water ~~vapor~~ (which represents the sum of water vapor, liquid water, cloud ice, rain, and snow in a column extending from the surface of the Earth to the top of the atmosphere), total precipitation ~~(TP), vertical~~, vertically integrated moisture divergence ~~(VIMD),~~, mean sea level pressure (MSLP), ~~and~~ 10-meter zonal and meridional wind components, daily radiative fluxes of shortwave and longwave radiations, (denoted as Q_{SW} and Q_{LW} respectively), and turbulent heat fluxes of latent and sensible flux (denoted as Q_{lat} and Q_{sen} respectively) were retrieved from the ERA5 reanalysis (Hersbach et al., 2020). The surface net heat flux (Q_{net}) was derived from a combination of radiative and turbulent fluxes (Menna et al., 2023).

$$Q_{net} = Q_{SW} - Q_{LW} - Q_{lat} - Q_{sen} \quad \text{.....(1)}$$

High-resolution SLA observations were obtained from the SWOT Level 3 satellite product, which offers 2 km spatial resolution, provided by Archiving, Validation and Interpretation of Satellite Oceanographic data (AVISO; https://www.aviso.altimetry.fr/en/data/products/sea-surface-height-products/global/swot-l3-ocean-products.html).

Lastly, biogeochemical ~~parameters~~variables such as chlorophyll, phytoplankton, nutrients, and dissolved oxygen were accessed via the CMEMS from the product MEDSEA_MULTIYEAR_BGC_006_008, available at a 4-5 km spatial resolution, and 1-hr temporal resolution (~~https://doi.org/10.25423/cmcc/medsea_multiyear_bgc_006_008_medbfm3).~~https://doi.org/10.25423/cmcc/medsea_multiyear_bgc_006_008_medbfm3). Daily satellite-derived chlorophyll products (OCEANCOLOUR_MED_BGC_L4_NRT) with ~~1 km~~a spatial resolution ~~have also been~~of 1 km were used in this study (Volpe et al., 2019; Volpe et al., 2018; Berthon ~~et al.,~~and Zibordi, 2004~~), which~~). These datasets are archived ~~from~~by the Copernicus Marine Service (~~https://doi.org/10.48670/moi-00298).~~ https://doi.org/10.48670/moi-00298) and are provided by the Italian National Research Council (CNR, Rome, Italy), with data availability from January 2023 to the present. The multi-sensor product integrates observations from SeaWiFS, MODIS, MERIS, VIIRS, and OLCI, and includes key biogeochemical variables such as chlorophyll-a (Chl-a), diffuse attenuation coefficient at 490 nm, and primary production.

~~**3.2 Methods:** In this study, we investigate medicane Daniel. A detailed description of the event and the methodologies employed in the analysis are provided below.~~

Despite their advantages, these datasets are subject to uncertainties arising from atmospheric correction errors, cloud contamination, aerosol effects, and reduced accuracy in optically complex coastal waters. In addition, the gap-filling procedure used to generate continuous fields may introduce smoothing in regions with persistent data gaps. Nevertheless, these products provide robust, high-resolution information on surface biogeochemical variability associated with cyclone-induced ocean processes.

3.2 Methods: In this study, we investigate the intensification, structure, and impacts of medicane Daniel. This section outlines the methodologies used to analyze the oceanic and atmospheric conditions associated with the event. The analysis focuses on key processes influencing cyclone formation and intensification, including the role of oceanic features such as WCEs and marine heatwaves, the contribution of ocean heat content as a source of subsurface thermal energy, and atmospheric variables such as moisture and wind fields. The methods used for the identification of the sea eddies and MHWs, as well as the computation of ocean heat content, are described below.

3.2.1 Eddy and ~~Marine Heat Wave (MHW)~~marine heatwave identification:

Eddy identification in this study followed the approach of Jangir et al. (2021, 2023) and Sun et al. (2017), based on geostrophic balance equations relating SLA to geostrophic currents. ~~Zonal~~zonal (u) and ~~Meridional~~meridional (v) velocity components were derived using equations 2, 3, and 4:

$$u = -\frac{g}{f}\left(\frac{dh}{dy}\right) \quad \text{.....(2)}$$

$$v = \frac{g}{f}\left(\frac{dh}{dx}\right) \quad \text{.....(3)}$$

$$V^2 = u^2 + v^2 \quad \text{~~.....(~~.....(4)}$$

~~where u and v are the zonal and meridional components,~~where g is the acceleration caused by gravity, f is the Coriolis parameter, h is the SLA, and V is the geostrophic current speed.

Eddies were classified by analysing flow circulation and SLA patterns: anti-cyclonic circulation with a local SLA maximum indicated ~~WCEs~~a WCE, while cyclonic circulation with

a local SLA minimum indicated a cold-core ~~eddies (CCEs~~eddy (CCE). This is consistent with previous findings, where WCEs in the Northern ~~Hemisphere~~hemisphere exhibited clockwise (anti-cyclonic) rotation, while CCEs rotated counterclockwise (cyclonic). The relation between anti-cyclonic eddies and WCEs along the cyclone's path was also verified by inspecting SST anomalies with respect to a boxcar average.

MHWs were identified using the definition by Hobday et al. (2016) and the software developed by Zhao et al. (2019) (https://github.com/ZijieZhaoMMHW/m_mhw1.0). An MHW is defined as a period of at least five consecutive days during which the daily SST exceeds the seasonally varying 90th percentile, based on a climatological reference period (1983–2021). Events separated by less than three days are treated as a single MHW. Daily SST anomalies were computed by subtracting the daily climatology. MHW intensity was classified following Hobday et al. (2018) into four categories based on the metric θ, where ~~θ moderate ($1 \leq \theta \leq 2$), strong ($2 \leq \theta \leq 3$), severe ($3 \leq \theta \leq 4$), and extreme ($\theta \geq 4$).~~ represents the normalized SST anomaly relative to the climatological threshold. It is defined as:

~~Where~~

$$\theta = \frac{SST - SST_{climatology}}{SST_{90th\ percentile} - SST_{climatology}} \quad \frac{SST - SST_{climatology}}{SST_{90th\ percentile} - SST_{climatology}} \qquad \text{.....(5)}$$

where SST is the daily sea surface temperature, $SST_{climatology}$ is the climatological mean SST, and $SST_{90th_{percentile}}$ is the seasonally varying 90^{th} percentile threshold. Based on this metric, MHW intensity is categorized as follows: moderate ($1 \leq \theta \leq 2$), strong ($2 \leq \theta \leq 3$), severe ($3 \leq \theta \leq 4$), and extreme ($\theta \geq 4$).

3.2.2 Computation of ~~Ocean Heat Content~~ocean heat content

We have also calculated the OHC to assess the role of subsurface heat accumulation in driving compound extreme events, such as the co-occurrence of MHWs and cyclones. Since the ocean acts as a key energy source for cyclones by supplying heat and moisture, the passage of a cyclone typically extracts heat from the upper ocean, leading to a decrease in OHC. In this study, OHC is defined as the vertically integrated thermal energy from the surface down to the depth of the 20 °C isotherm (a proxy for the thermocline layer). The OHC was computed for the medicane using the following formulation (Equation 6):

$$OHC = \int_{h1}^{h2} \rho C_p \, T dz \quad \text{.....(6)}$$

where ρ is the density of the seawater, C_p is the specific heat capacity of the seawater at constant pressure, *p*, *h1* is the surface, *h2* is the bottom depth, and *T* is the temperature in °C. This approach allows us to quantify how much thermal energy is available in the upper ocean to potentially intensify cyclones and how this energy is depleted following cyclone passage.

3.2.3 Computation of Ekman pumping

Ekman pumping was computed using the wind stress components $\tau=(\tau_x, \tau_y)$ from ERA5, namely Eastward Wind Stress (EWSS) and Northward Wind Stress (NSSS~~).~~), which is available for 0.25° × 0.25° and hourly temporal resolution. To compute the wind stress curl (∇×τ), the spatial derivatives of wind stress are used, and it is computed using equation 7:

$$curl(\tau) = \frac{\partial \tau_y}{\partial x} - \frac{\partial \tau_x}{\partial y} \quad \text{.....(7)}$$

The wind stress curl (∇×τ) was calculated using finite-difference estimates of spatial gradients on a latitude-longitude grid, with grid spacing converted to metric units. No additional smoothing was applied to the wind stress fields prior to curl computation. Then, the Ekman pumping velocity (w_e), introduced by Stern (1965) to account for the effect of the ocean currents on upwelling, is calculated using equation 8:

$$w_e = \frac{1}{\rho(f+\zeta)} \times \frac{1}{\rho} \times curl(\tau)$$

$$\text{.....}\left(\frac{\tau}{f+\zeta}\right)\text{.....(8)}$$

This vertical velocity reflects the upwelling (positive w_e) or downwelling (negative w_e) of water, and is a crucial mechanism through which cyclones influence oceanic nutrient transport, mixing, and biological productivity~~.~~ (Li et al., 2021). Here, the relative vorticity (ζ) was computed from the zonal (u) and meridional (v) components of the surface current, as given in Equation (9):

$$\zeta = \frac{\partial v}{\partial x} - \frac{\partial u}{\partial y} \text{.....(9)}$$

The Ekman transport vector components were computed from the wind stress and Coriolis parameter as:

$$M_x = \frac{\tau_y}{\rho f} \quad \left(\frac{\tau_y}{\rho(f+\zeta)}\right) \quad (10)$$

$$M_y = \frac{\tau_x}{\rho f} \quad \left(\frac{\tau_x}{\rho(f+\zeta)}\right) \quad (11)$$

where ρ is seawater density, and f is the Coriolis parameter (dependent on latitude). The vector field M=(M_x , M_y) was visualized using quiver plots to reveal the spatial structure and directional response of Ekman transport to cyclone wind forcing.

~~**4. Results and Discussion**~~

~~***4.1 The presence of ocean features i.e., Eddies, Marine Heat Wave and Ocean Heat Content along the cyclone track and their Impact on cyclone intensity***~~

3.2.4 Computation of various properties along the track of medicane Daniel

To estimate medicane's characteristic MSLP and wind speed along the cyclone track, we applied Cressman averaging (Cressman, 1959). Once the cyclone center was identified, a spatial average within a 2° radius around the center, weighted by inverse square distance, was computed for MSLP and wind speed. This method captures changes within a 2-degree radius of the cyclone centre, while regions outside this radius are not included. Similarly, daily MHW and high-pass filtered (500 km radius) SST and OHC anomalies, along with their along-track evolution during Cyclone Daniel where calculated using the 2-degree search radius and the Cressman interpolation technique. This analysis allows quantification of the relative extremity of the oceanic conditions encountered during intensification. The approach was used to assess variations in cyclone intensity along its path and has been widely employed in previous studies (Jangir et al., 2023).

4. Results and discussion

In this section, we present the results of our study on medicane Daniel, focusing on two primary aspects. First, we analyze the influence of pre-existing oceanic conditions, specifically WCEs and MHW conditions, on the cyclone's intensification. Second, we investigate the medicane's

impact on ocean biogeochemistry, particularly the observed increase in surface productivity as indicated by enhanced biogeochemical variables. Our findings also explore the physical mechanisms behind these changes, highlighting the interactions between the ocean and atmosphere throughout the lifecycle of medicane Daniel.

4.1 Role of oceanic features in intensification of medicane Daniel

Figure 1a~~, -~~b shows the SLA along the ~~cyclone's~~medicane's track. At first, the medicane passed over a cluster of three ~~anti-cyclonic WCEs~~anticyclonic eddies between September 4 and 6, presumably contributing to its intensification (Jangir et al., 2023). This intensification ~~is~~between 8 and 10 September was also supported by the presence of a moderate MHW, as shown in Figure 1c–e (see also SI Figure 1~~), which reveals~~). Furthermore, just before making landfall, the medicane arrived in a ~~moderate MHW at~~ region characterized mostly by anticyclonic mesoscale WCE activity (figure 1f–h). OHC anomaly shown in Figure 1i–k indicates higher heat content in the southern part of the domain close to landfall location, also supporting the intensification ~~location~~of the medicane. In addition to the maps in panels c–k of Figure 1, the analysis was carried out by computing MHW, SST, and OHC anomalies at each 6-hourly track position (Figure 1l-n), with particular emphasis on ~~9 September 2023.~~ the maximum cyclone intensity (Max-CI) location. We observed from the analysis that the maximal values of MHW, SST, and OHC anomalies occurred in the last two days before Max-CI, indicating that medicane Daniel intensified over thermodynamically favourable conditions that were among the most anomalous along its track.

The ~~presence~~combination of two extreme ~~conditions~~oceanic preconditions, namely the WCE and ~~MHW,~~the MHW, together with high absolute values of OHC at the intensification site near the coastal region, may have contributed to ~~making~~ the deadly outcome of this ~~the deadliest cyclone recorded in the MS (Figure 1).~~medicane. Rathore et al. (2022) and Jangir et al. (2024) highlighted the critical role of sudden intensification in Cyclone Amphan over the Indian Ocean and medicane Ianos over the ~~MS~~Mediterranean Sea, respectively, in the presence of MHWs along their paths. The findings of the current study are consistent with these observations, demonstrating that while cyclone genesis and intensification can occur independently of such features, the presence of WCEs and MHWs ~~can significantly~~may enhance the rate and magnitude of intensification over a shorter time.

~~Figures~~Figure 1 ~~mainly~~also highlights the potential importance of ocean characteristics such as WCEs and MHWs in cyclone intensification, indicating that cyclone intensity increased in the presence of WCEs and MHWs. This behavior is similar to how cyclones in other ocean basins react to changes in intensification factors related to underlying eddies (Ali et al., 2007; Lin et al., 2013; Jangir et al., 2020; Jangir et al., 2023). When a cyclone encounters a WCE, the negative feedback loop between cyclone intensity and SST diminishes. Normally, cyclones ~~absorb~~extract heat from the ocean, ~~causing~~resulting in surface cooling ~~through~~due to enhanced mixing and evaporation, ~~reducing their~~which acts to reduce cyclone intensity. However, if a WCE or ~~MHW is~~marine heatwaves are present, the high SST persists longer, intensifying the cyclone and reducing the negative feedback effect (Bender et al., 1993; Jangir et al., 2024).

Furthermore, ~~Cyclones also~~atmospheric cyclones draw a significant portion of their energy from warm, deep ocean waters; therefore, quantifying the amount of this warm, deep water provides a more accurate measure of the energy available to the storm. OHC serves as this metric, indicating how much warm water a cyclone can convert into energy. Studies have shown that OHC is a far superior predictor compared to SST alone (Wada & Usui, 2007; Sharma and Ali, 2014; Lin et al., 2013; Law et al., 2011). Analysis of the OHC revealed ~~that there is~~ a significant amount of OHC at the intensification locations, providing the energy necessary for medicane Daniel to intensify. Approximately 120 KJ/cm² of heat was available from September 4th to 9th, even before the cyclone's intensification (Figure ~~1f-h~~1i-k & SI Figure 2). This accumulated heat at the intensification location is attributed to the presence of the warm-core eddy and the ~~MHW~~marine heatwave, which decreases after the passage of the medicane on the 11th and 12th of September, 2023 (SI Figure 2). The presence of ~~the accumulated~~ heat in the form of SST anomaly (Figure 1f-h) and OHC anomaly (Figure 1i-k) along the path of medicane maintains intensity by reducing negative feedback that occurs due to the passage of the cyclone (Jangir et al., 2023; Jangir et al., 2024).

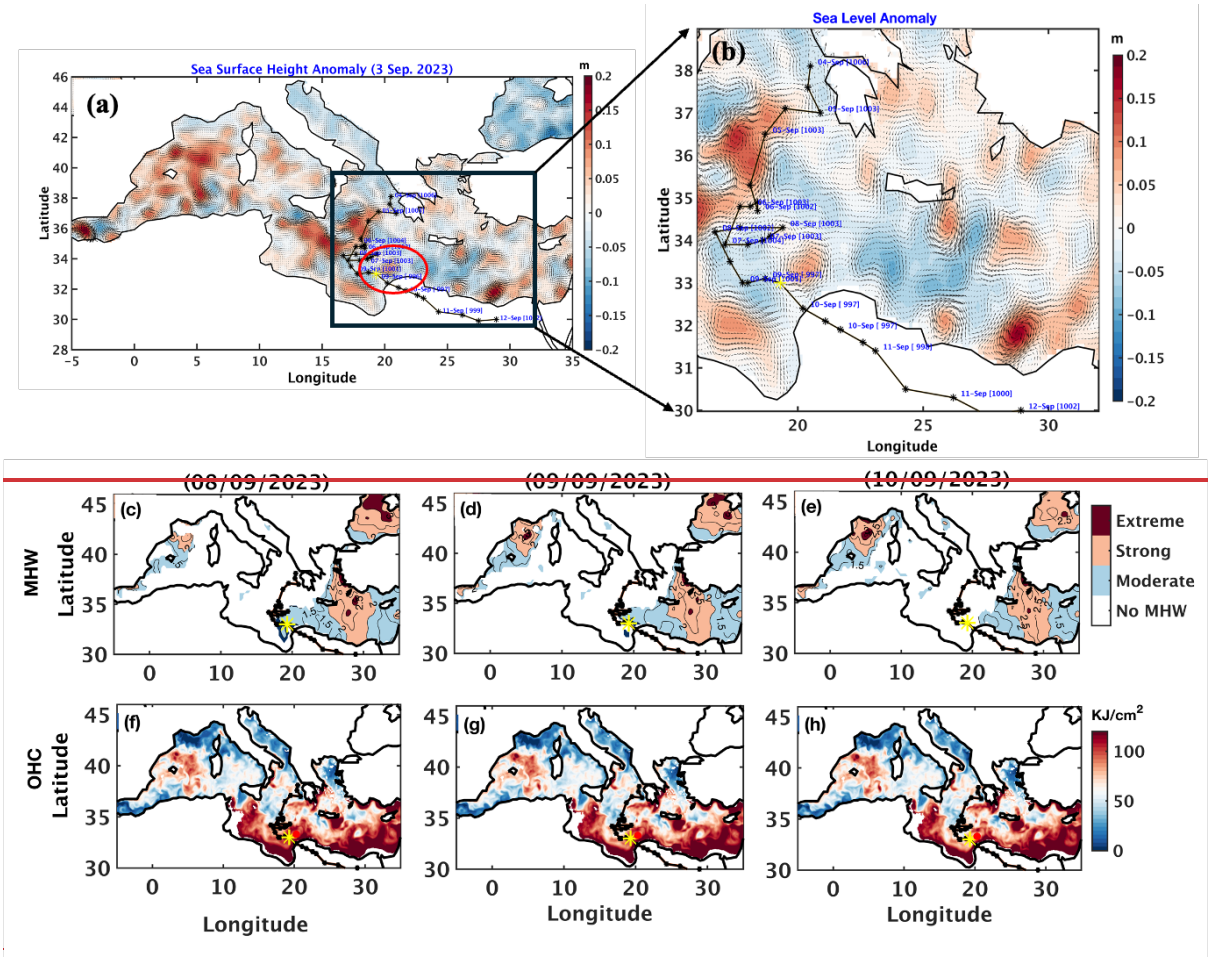
Sea Surface Height Anomaly (3 Sep. 2023)
(a)
Latitude
Longitude
m
Sea Level Anomaly
(b)
(08/09/2023)
(09/09/2023)
(10/09/2023)
(c)
(d)
(e)
(f)
(g)
(h)
MHW
OHC
Extreme
Strong
Moderate
No MHW
KJ/cm2

442

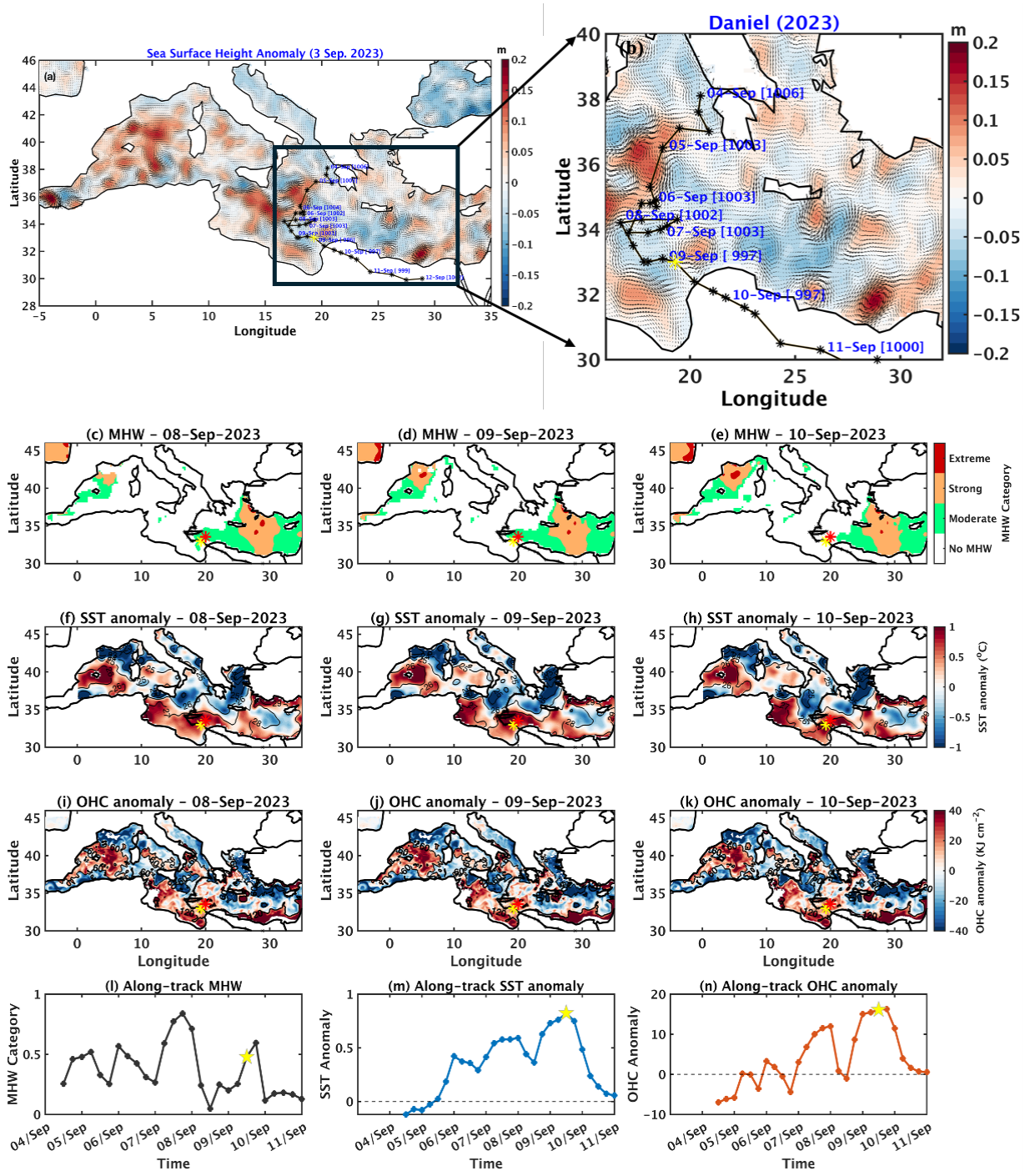

Figure 1: (a, b) Sea level anomaly ~~in (~~shading ~~and)~~ with geostrophic currents ~~(~~arrows~~,~~ ~~Medicane).~~ The medicane track is overlaid on (c~~,e) Marine Heat Wave~~-e) marine heatwave (MHW), (f-h) sea surface temperature (SST) anomalies (500 km radius high pass filter), and (i-k) ocean heat content (OHC) anomalies (500 km radius high pass filter). In panels f-k, absolute values are indicated by contours. Panels (l-n) show along-track values of MHW, SST, and ~~(f,h) Ocean Heat Content, Yellow star represents~~OHC anomalies. The yellow stars (pentagon) in panels a-k (l-n) mark the ~~intensification~~ location ~~and~~ of maximum cyclone

intensity (Max-CI), while the red ~~*dot on Ocean Heat Content showing*~~*pentagons mark* the *Max-CI* location ~~*of*~~ *defined by the minimum mean sea level pressure. The red star marker in panels c-k indicates the position of the WCE. Dates for each panel are shown along the track.*

4.2 The role of ~~Atmospheric Precursors~~atmospheric precursors in the ~~Intensification~~intensification of ~~Medicane~~medicane Daniel

The MSLP~~,~~ and wind speed ~~(WS), and net heat flux (NHF) along the cyclone's track are shown in Figure 2a. The MSLP~~, computed using the Cressman averaging method (Cressman, 1959~~),~~) along the cyclone's track, are shown in Figure 2a. The MSLP indicates moderate intensification for 1006 hPa to 1002 hPa when the storm passes over the WCE on 5 September 2023 (Figure 2a). Subsequently, from the 6th to the 7th September 2023, the medicane passes over a CCE region, and its intensity is reduced to 1004 hPa. Upon reaching the vicinity of Libya's coast on ~~the 8th~~8 September 2023, it quickly ~~intensifies~~intensified. An additional WCE was present in the vicinity of the cyclone's path at that time, potentially further contributing to its fast intensification. This fast intensification is indicated by a drop in the MSLP and a sudden increase in ~~WS~~wind speed near the eddy and MHW location (Figure 2a). ~~Figure 2a shows that on September 7, 2023, the MSLP was 1003 hPa. Upon reaching the vicinity of the eddy, the MSLP dropped by 6 hPa to 997 hPa (Figure 2a) in 12 hours, and significant NHF were released at the cyclone's intensification location (Figure 2b-d and SI Figure 3), providing the energy necessary for the cyclone to intensify.~~ The cutoff low, which was supported by high net heat flux, persisted for two days (Figures 2b-d, SI Figure 3), even after the cyclone made landfall in Libya~~, resulting in significant damage along the Libyan coast~~.

Moisture processes play an equally important role in cyclone intensification. Their ~~significane has~~importances been demonstrated in previous studies by Jangir et al. (2023) and Pytharoulis et al. (2018), emphasizing that elevated SST in the form of ~~eddy~~WCE or MHW is essential ~~in~~for providing moisture to a medicane via surface fluxes, enhancing convection. Additionally, Jangir et al. (2024) highlighted the importance of ~~-~~moisture convergence in the intensification of cyclones and increasing total associated precipitation. Thus, motivated by these findings, we focus in this study ~~we mainly focus~~ on the ~~cause~~causes of the intensification of the medicane Daniel and the extreme flood that occurred during the event.

The analysis of moisture convergence (i.e., mean vertically integrated moisture divergence) showed a pattern of moisture convergence along the cyclone's path. Notably, this convergence

coincides with the eddy location at the intensification location on September 9th, 2023 (SI Figure 4). This alignment suggests that the eddy supplied the moisture needed for the cyclone's intensification. The interaction between the eddy and the medicane likely enhanced moisture availability, contributing to the storm's strengthening at that specific point in ~~its~~it's path. Additionally, the total column water was notably high at the ~~eddy~~WCE and MHW locations. While this total water was present before the intensification location as well, it converged around the eddy at the intensification location (SI Figure 5), leading to substantial precipitation in that area (Figure 2e-g and SI Figure 6). The severe precipitation near the coastal region~~,~~ ~~primarily due to the presence of a WCE and MHW, significantly contributed to the extensive destruction along the Libyan coast.~~ highly coincides with the WCE and MHW. The WCE's influence intensified the cyclone by providing additional moisture and heat, leading to heavy rainfall. This heavy precipitation, concentrated near the coast, exacerbated the storm's impact, severely damaging the affected areas.

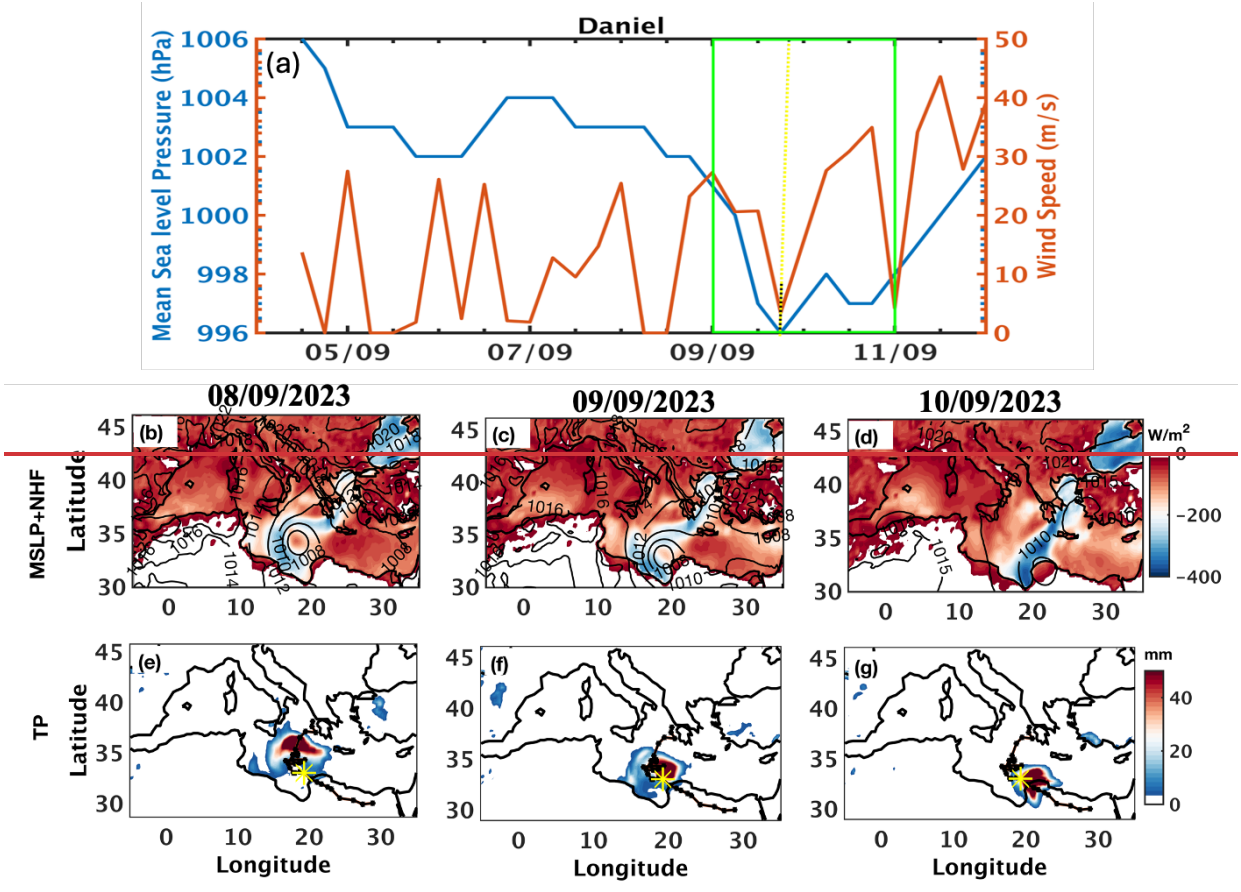

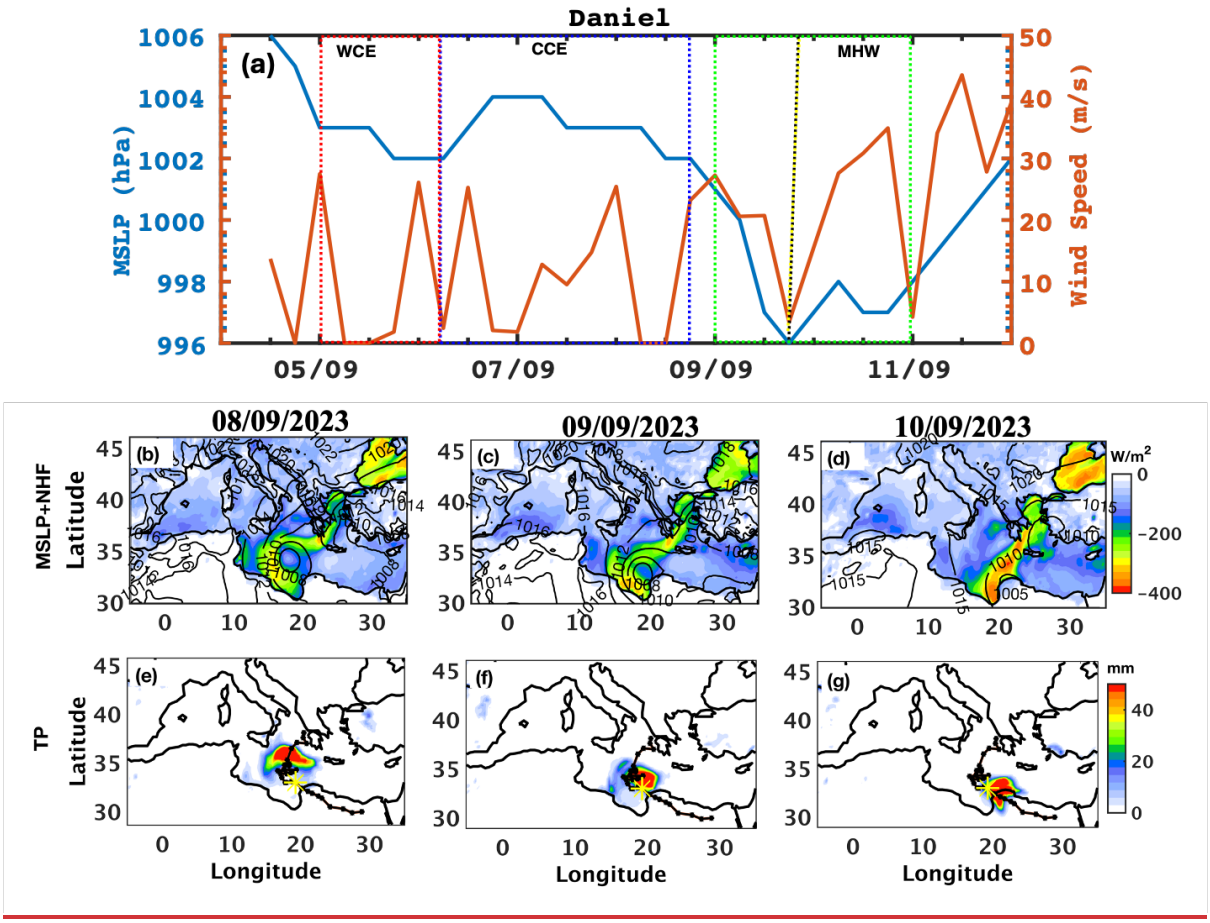

Figure~~:~~ 2~~:~~ (a) Mean sea level pressure~~,~~ (MSLP), and wind speed~~, and net heat flux~~ computed using the Cressman average along the track of the medicane Daniel. ~~Medicane~~The red, blue, and green boxes indicate the locations of the warm-core eddy, cold-core eddy and marine heatwave, respectively. The medicane track is overlaid on (b-d) ~~Contours of~~ the daily mean of MSLP ~~overlaid on the daily mean of latent~~(contours) net heat fluxes (shading; positive downward), and on (e-g) total precipitation ~~during the cyclone, on the 8th, 9th and 10th~~for 8-10 September 2023. ~~Yellow~~The yellow star ~~represents~~indicates the location of maximum intensification ~~location.~~(Max-CI).

4.3 ~~Use of~~ SWOT satellite data ~~in cyclone studies in the Mediterranean Sea~~

The SWOT mission offers high-resolution sea surface height anomaly (SSHA) or SLA data with unprecedented spatial detail, enabling precise detection of mesoscale and sub-mesoscale ocean features, such as eddies and fronts (Morrow et al., 2019). This can be valuable for studying cyclones, which interact strongly with oceanic eddies that influence storm intensity. Unlike traditional altimeters, SWOT's wide-swath coverage ~~captures fine-scale structures generated by cyclone-induced mixing.~~ enables improved detection of mesoscale and sub-

mesoscale eddies, frontal gradients, and filaments that regulate ocean heat distribution and air-sea exchanges. These features are often underrepresented in low-resolution datasets, limiting their ability to capture localized processes such as eddy-cyclone interactions and cyclone-induced mixing. By resolving these fine-scale physical structures, SWOT also provides a framework for interpreting biogeochemical responses. While coarse datasets show bulk chlorophyll changes, SWOT helps identify localized regions of enhanced mixing and upwelling that drive nutrient supply and biological variability. This allows for a clearer linkage between physical forcing and biogeochemical response. Overall, SWOT overcomes key limitations of conventional altimetry by preserving high-frequency spatial gradients, enabling a more accurate representation of the ocean state during extreme events such as medicane Daniel.

Here we show the SWOT swath passing over the location of the eddies along the track of medicane Daniel (Figure 3). In Figures 3a ~~and 3b~~ b, the eddy initially appears small and low intensity in the CMEMS, and the cyclone is observed nearby. However, SWOT data ~~reveals~~reveal a more intense and extensive eddy structure than CMEMS, with the cyclone positioned directly above it. ~~Notably, Figure 3e shows a high post-cyclone increase in Chl-a concentration over both the eddy locations. Complementary to this, Figure 3 indicates enhanced Ekman pumping roughly at the same locations, likely contributing to the observed Chl-a increment over both eddies.~~ These findings report the value of SWOT observations in capturing fine-scale oceanic features and dynamics, offering critical insights into cyclone-eddy interactions~~, vertical nutrient transport, investigating sub-mesoscale air-sea interactions, and improving coupled ocean-atmosphere models~~.

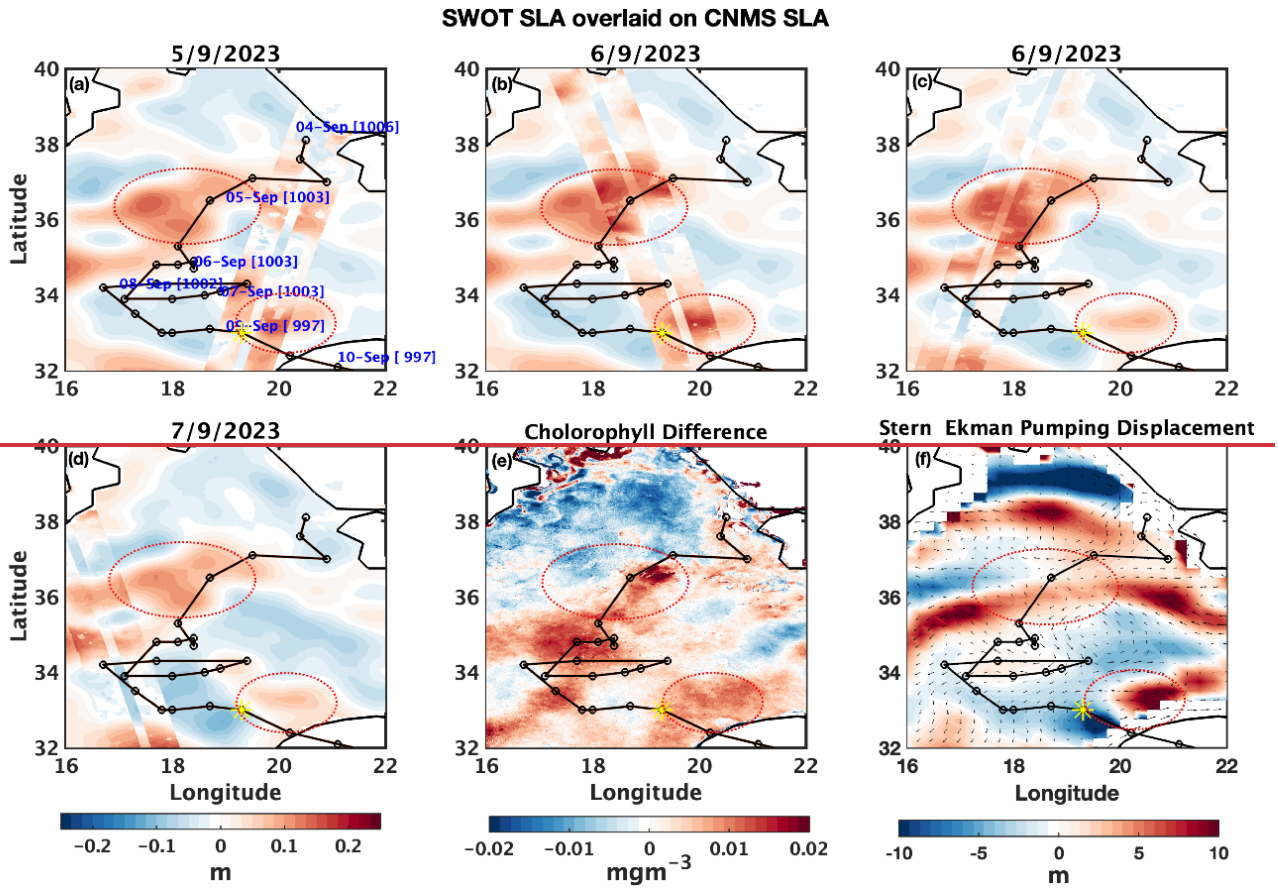
SWOT SLA overlaid on CNMS SLA
5/9/2023
6/9/2023
6/9/2023
7/9/2023
Cholorophyll Difference
Stern Ekman Pumping Displacement
(a)
(b)
(c)
(d)
(e)
(f)
04-Sep [1006]
05-Sep [1003]
06-Sep [1003]
08-Sep [1002]
07-Sep [1003]
09-Sep [997]
10-Sep [997]
Latitude
Longitude
m
mgm^{-3}

540

541

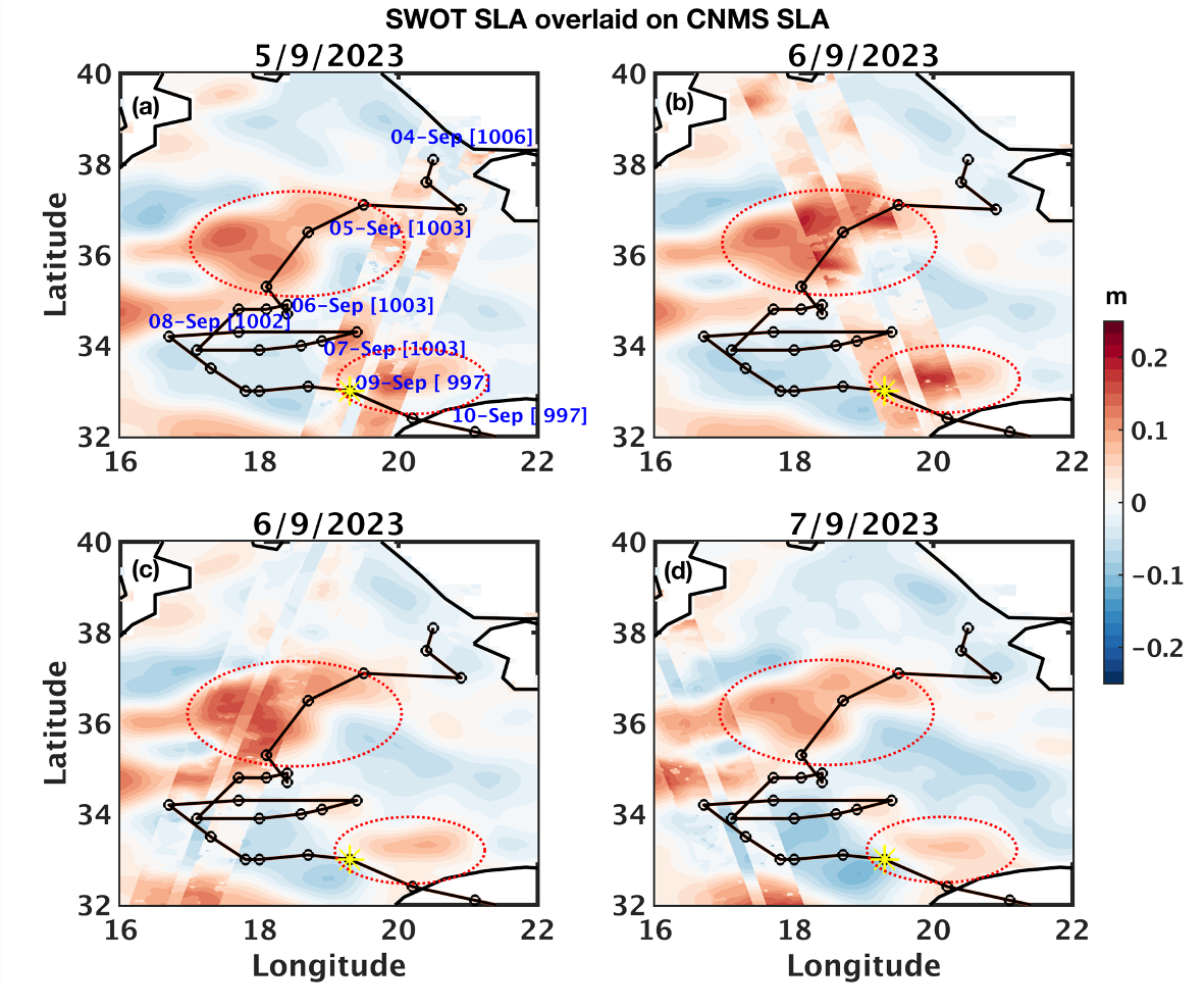

Figure 3: (a-d) The SWOT sea level anomaly (SLA) swath (~~with~~2 km resolution ~~2 km~~) overlaid on SLA from CMEMS (12.5 km spatial resolution). ~~(e) Satellite chlorophyll (2 km spatial resolution) before and after Storm Daniel. (f) Average (5-10 September 2023) Ekman pumping displacement and arrows of transport vector during~~The dates shown above each panel correspond to the ~~cyclone~~ periods of SWOT swath data availability.

4.4 Impact of medicane Daniel on ocean biogeochemistry

To investigate the impact of the medicane on oceanic physical (temperature and salinity) and biogeochemical properties~~,~~ (i.e., chlorophyll-a, phytoplankton, nitrate and phosphate, and oxygen concentration), we analyzed vertical profiles of key variables along the cyclone's track. The analysis focused on differences between two days after the cyclone's passage, minus two days before (Figure 4a-g). The results reveal a notable decrease in temperature along the cyclone path, with ~~the strongest~~a general strong cooling ~~observed near~~along its path except for a short pause in the cold SST anomaly region in the ~~WCE~~morning of the 8th (Figure 1n). This region was also relatively outside the MHW domain (Figure 1l). The salinity also decreases on the surface presumably due to a massive influx of freshwater from heavy rainfall, again,

except for the morning of the 8th, in which the cyclone was outside the influence of warm-core eddies and ~~MHW locations.~~marine heatwave (Figure 4b). In contrast, at the subsurface, Chl-a and phytoplankton concentrations ~~at the surface~~ exhibit a marked dipole ~~at the subsurface.~~(Figure 4c-d), while nutrients increase (Figure 4e-f) and oxygen decreases (Figure 4g). This biological response ~~is~~can be attributed to cyclone-induced Ekman pumping upwelling and high subsurface vertical mixing. Enhanced nutrient availability at the subsurface layer ~~allows~~can persist into the mixed layer, allowing for sufficient sunlight, and together with elevated oxygen concentrations~~,~~ (associated with surface cooling), may foster increased surface Chl-a and phytoplankton biomass. Signs of this can be seen in the MHW region, where higher Chl-a concentrations reach the surface. But, unlike previous results (Jangir et al., 2026), medicane Daniel only shows ~~a small~~an increase in Chl-a at the surface in the MHW region.

Profiles of temperature and Chl-a at the maximum cyclone intensity (Max-CI) location and time (Figure 4h~~, -~~i) reveal ~~that~~general cooling after the ~~DCM~~passage of the cyclone. The deep chlorophyll maximum (DCM) was located far below the ~~MLD~~mixed layer depth, at around 140m depth. ~~We already know that cyclone-induced upwelling was negative there (Figure 3f), indicating downwelling, so it cannot explain the increase in Chl-a at the surface. The profiles in Figure 4i are in agreement with the downwelling, showing a small decrease in the DCM depth.~~ The subsurface crossings between the profiles ~~in this figure~~ and the relatively stationary location of the DCM in Figure 4i indicate that ~~a different mechanism was active, that is,~~out of the two processes mentioned above, namely cyclone-induced upwelling and high subsurface vertical mixing, only cyclone-induced subsurface mixing~~. This~~ can explain the change. Subsurface mixing mechanism is typically much slower than turbulence in the mixed layer, but under storm conditions may become comparable. The gradual subsurface increase in Chl-a, as opposed to the vertical line observed in the mixed layer, ~~suggests that subsurface~~ indicates weaker but comparable turbulence ~~is comparable to, but still weaker than, turbulence within~~below the mixed layer.

Figure 4i shows the change in subsurface profiles at the time and location of Max-CI, situated on the periphery of a WCE. To further investigate the underlying mechanisms and compare the medicane's impact on both WCEs and CCEs, vertical cross-sections ~~over~~across the main ~~WCE~~center of the WCE and adjacent CCE region were analyzed during the pre-storm, during storm, and post-storm phases (Figure 5). These cross-sections reveal notable eddy-dependent subsurface changes associated with the passage of the medicane. As expected, during and after

the passage of the storm, significant surface cooling is observed in Figure 5 (panels b-d and h-i). In addition to the cooling observed within the mixed layer, three distinct circular-like cooling patterns are evident immediately beneath it. These may indicate a secondary circulation ~~motion~~ starting at the deep ~~sub-surface~~subsurface (below 200m), which transfers deep cold water to the layers below the mixed layer. In this case, the two patterns on the right indicate an upwelling cell at the ~~WCE~~warm-core eddy boundaries (green arrows in Figure 5i) and another at the ~~CCE~~ cold-core eddy center~~.~~ (purple arrow in Figure 5i). These circulation cells also create the dipole pattern in the Chl-a ~~patterns of DCM upwelling~~ inside the WCE~~, but they do not explain the dipole pattern above the WCE.~~ and the CCE (Figure 5, panels e-g and j-k).

~~Figure 6 shows vertical profiles of Chl-a in two locations along the same line as in Figure 7a, one inside the CCE and one inside the WCE. These can guide us about the relevant active mechanisms. Inside the WCE, high Ekman pumping (Figure 3f) results in upwelling and upward shift of the DCM depth. Inside the CCE, Ekman pumping is less relevant - the DCM stays more or less at the same depth. Yet, the profiles in Figure 6a suggest that the dipole patterns inside the CCE in Figure 5k can be explained by subsurface mixing, which is stronger above the DCM. These observations suggest that although WCEs are generally associated with downwelling and reduced biogeochemical activity, the strong mixing and upwelling induced by the cyclone temporarily dominate this dynamic, leading to surface nutrient enrichment and increased biological activity. In the CCE, although the Ekman pumping is smaller (or negative), the higher DCM depth supports mixing of Chl-a to the surface through sub-surface mixing.~~

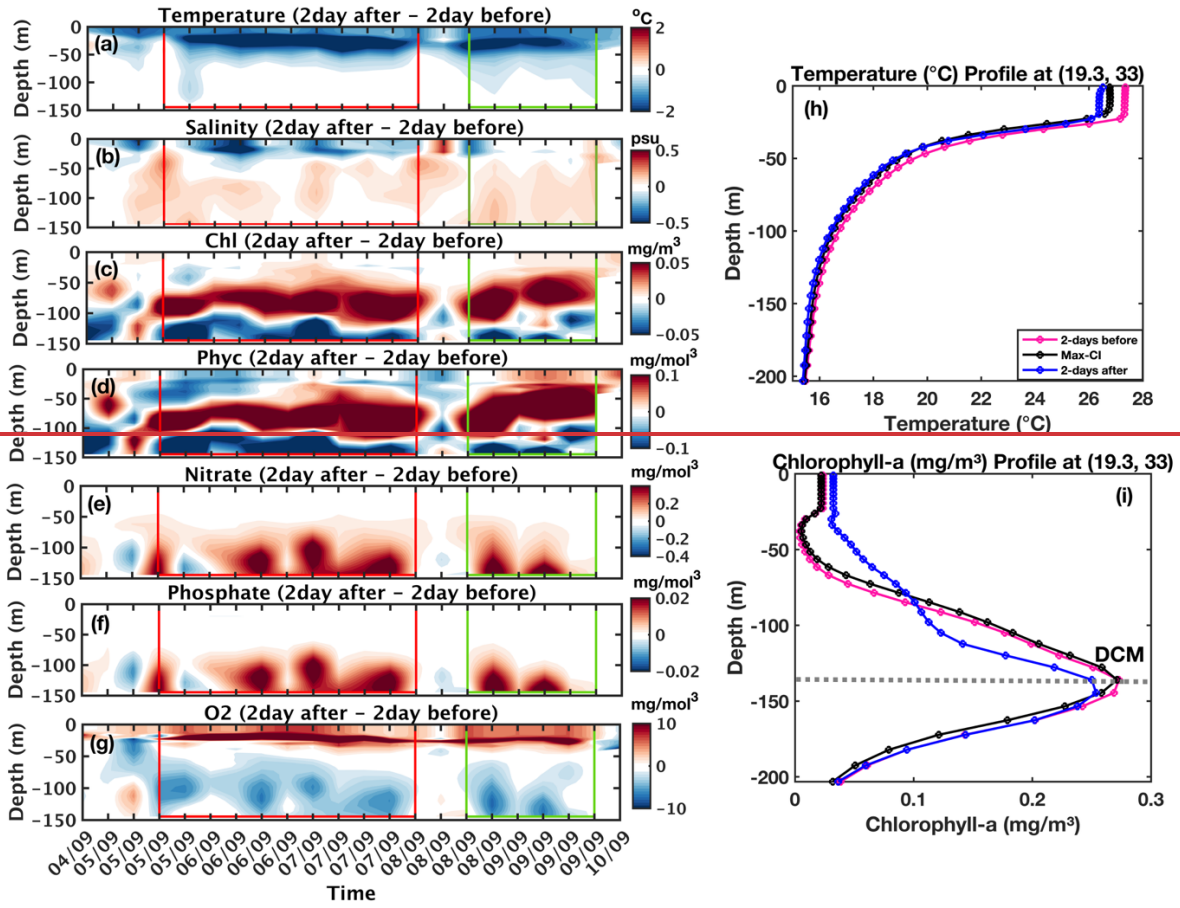

To explore the dynamical mechanisms, Figure 6 shows vertical profiles from 1 to 15 September 2023 of Chl-a at two locations along the same line as in Figure 5a, one inside the CCE (panel a) and the other inside the WCE (panel b). Before the arrival of the medicane (1-5 September), the DCM within the CCE was shallower than in the WCE, consistent with the typical vertical structure of these eddies. The DCM in both eddies remains relatively stable until the cyclone approaches the region. As the medicane approaches the eddies, it intensifies the CCE while diminishing the WCE, which, as expected from theory (e.g., Klein & Lapeyre, 2009), supports eddy-induced upwelling. Indeed, during the storm, the DCM is lifted upward in both cases from 5 to 9 September. Yet, the DCM inside the WCE is exhibited significantly greater shoaling than inside the CCE (~ 40m in the WCE relative to ~ 15m in the CCE). The more pronounced response in the WCE likely stems from lower thermal stratification and higher surface wind stress curl that contribute to cyclone-induced Ekman pumping upwelling. Only a few days later, the DCM inside the WCE partially starts to restore its pre-storm condition. The DCM inside the CCE quickly drops back down and even overshoots its depth relative to pre-storm conditions, which can be explained by its stronger stratification and resulting buoyancy restoring force. In addition, we found that cyclone-induced upwelling alone cannot explain the

DCM increase in both the WCE and CCE (Figure 6c), which indicates an increase of about 10-15 meters during the medicane influence (5-9 September). Therefore, we conclude that the upwelling may have also been influenced by isopycnal adjustment triggered by the medicane.

Subsurface mixing similar to what was shown under the medicane at Max-CI (Figure 4i), seems to play a role also here. This role can be indicated by the crossing of the Chl-a profiles during the storm (5-9 September) with the profiles after the storm (10-15 September) between MLD (~ -20m) and the DCM (~ -130m). However, here, it seems to complement upwelling and to play a more important role at the WCE (as expected, since in general wind stress is higher above WCEs). Also, satellite-based surface observations (Figure 6d) indicate higher Chl-a above the WCE region, which may be explained by the closer-to-the-surface DCM and stronger cyclone-induced upwelling and vertical mixing.

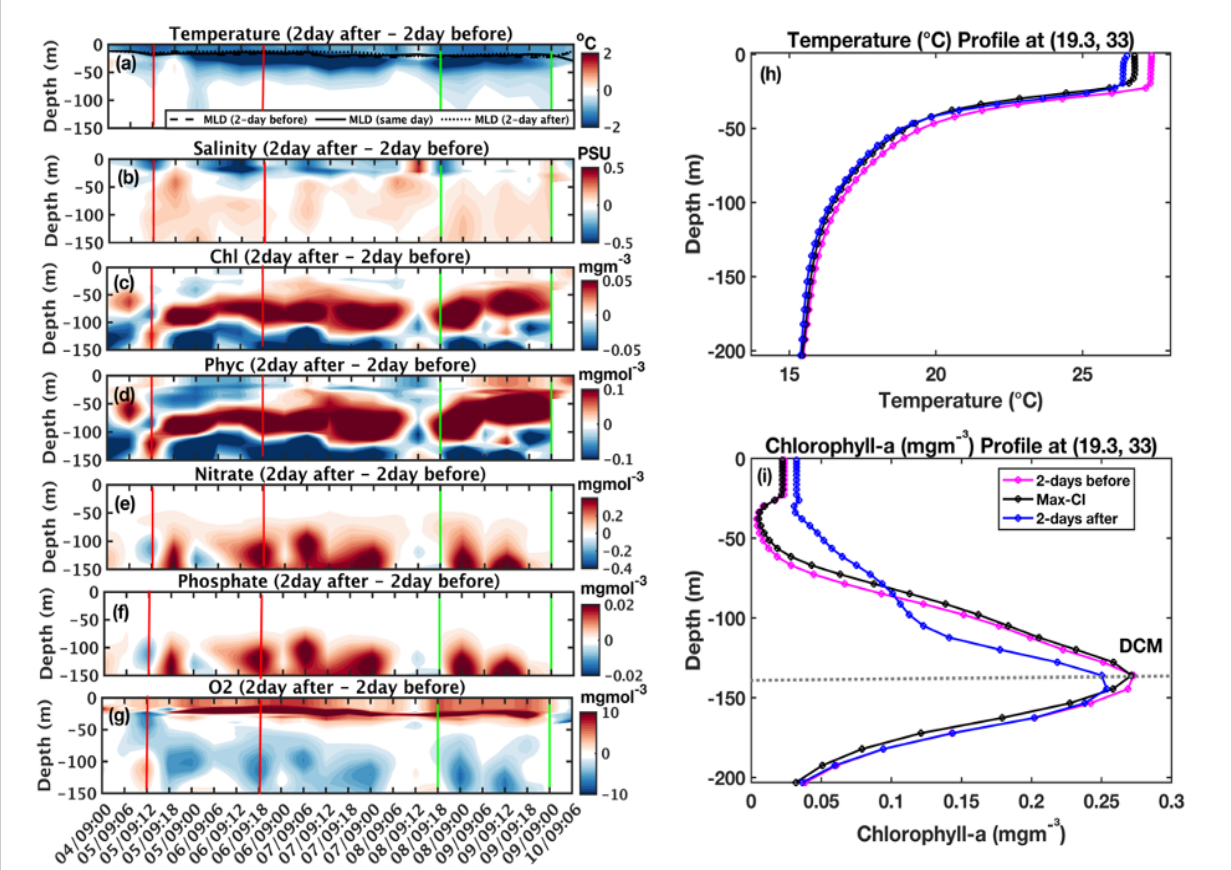

Figure 4: ~~Profile~~Profiles of physical (a-d) and biogeochemical (e-g) variables ~~(e-g)~~ along the ~~path~~track of ~~the cyclone~~medicane Daniel. The left panels ~~represent~~show the difference between two days after ~~the event minus~~ and two days before the event. ~~The red~~Red and green vertical lines in panels (a-g ~~bound~~) delineate the location of ~~MHW~~the warm-core eddy and

~~WCE~~marine heawave along the track ~~of the Mediterranean cyclone Daniel~~, respectively. The ~~vertical dotted~~ black ~~mark marks~~line in the ~~location of~~temperature profile indicates the ~~cyclone's maximum intensity~~mixed layer depth.

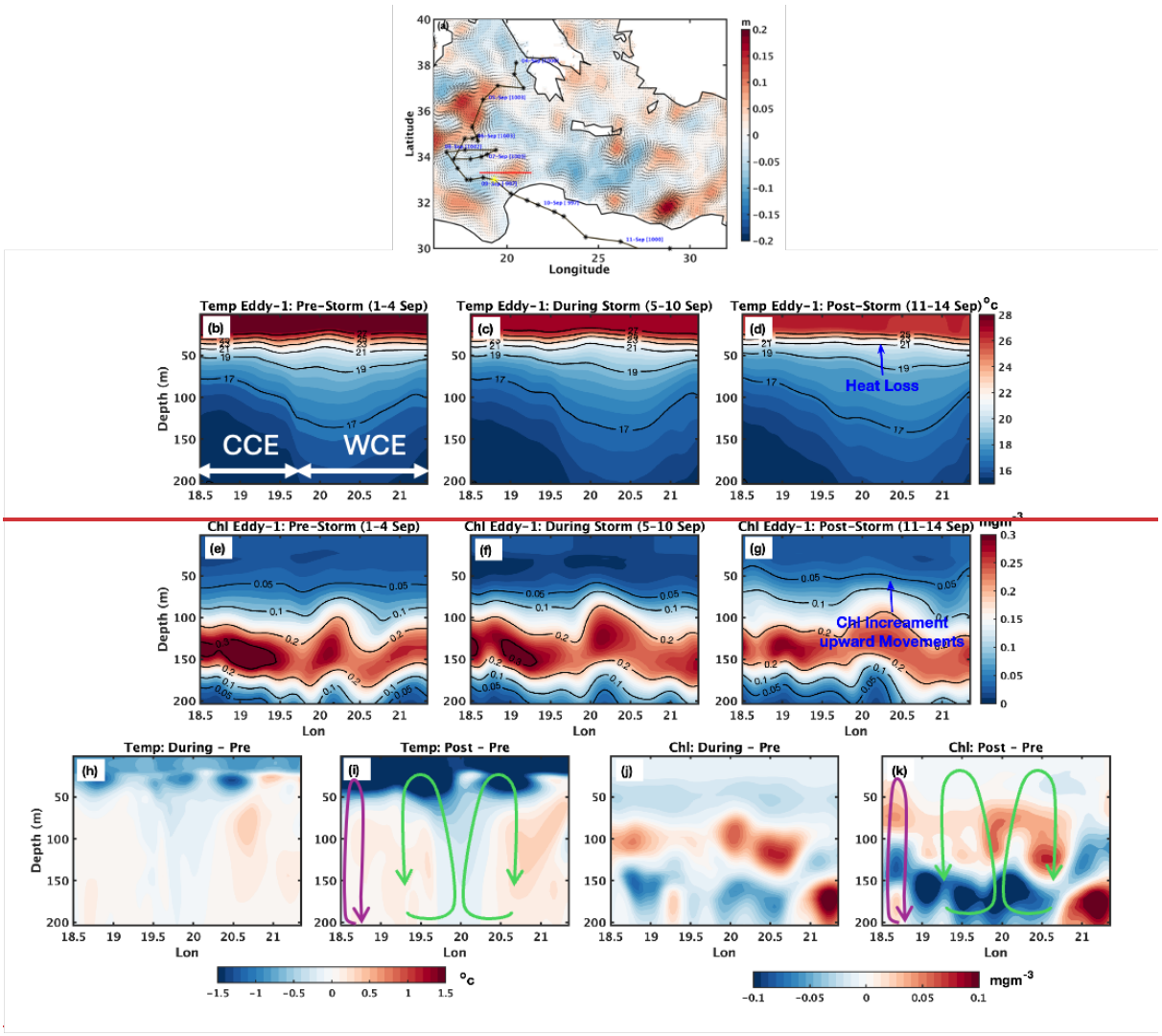

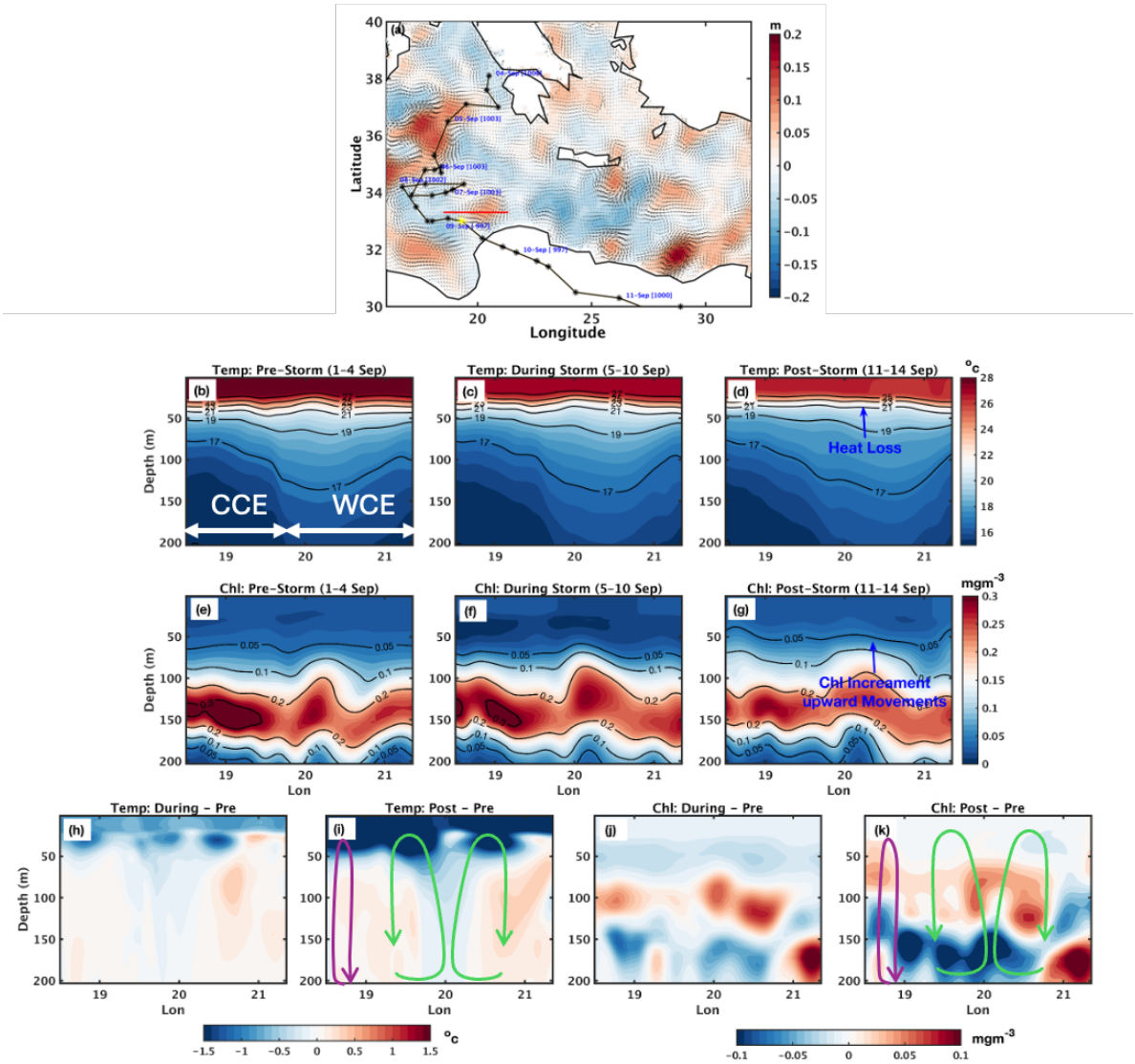

Figure 5: (a) Sea level anomaly ~~and~~with a red line ~~representing~~indicating the section ~~over~~across the second warm-core eddy (WCE~~, which is considered~~) used in ~~the next~~subsequent panels. (b-d) Temperature profiles and isotherms before, during, and after the medicane along ~~the~~this section~~ over the eddy.~~. (e-g) Chlorophyll-a profiles before, during, and after the medicane along the same section~~ over the eddy.~~. (h-i) ~~The difference in temp~~ Temperature differences (during-storm minus pre-storm, and post-storm minus pre-storm~~.~~). (j-k) ~~are the same~~Same as (h-~~j~~)i), but for ~~Chl~~Chlorophyll-a. Green arrows ~~represent~~denote the ~~estimated~~ location of a secondary circulation cell, and the purple arrow indicates subsurface mixing.

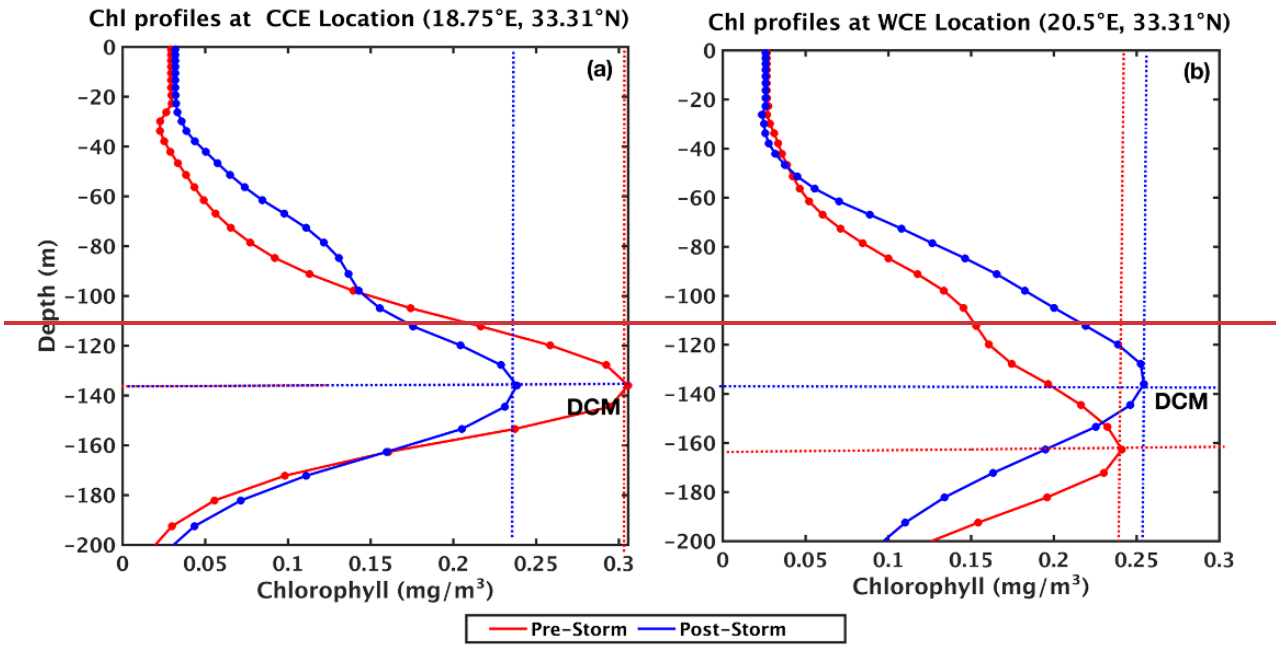

~~Figure 6: The Chlorophyll profiles before the storm (1–4 September), and after the storm (11–14 September) at the CCE location and WCE location.~~

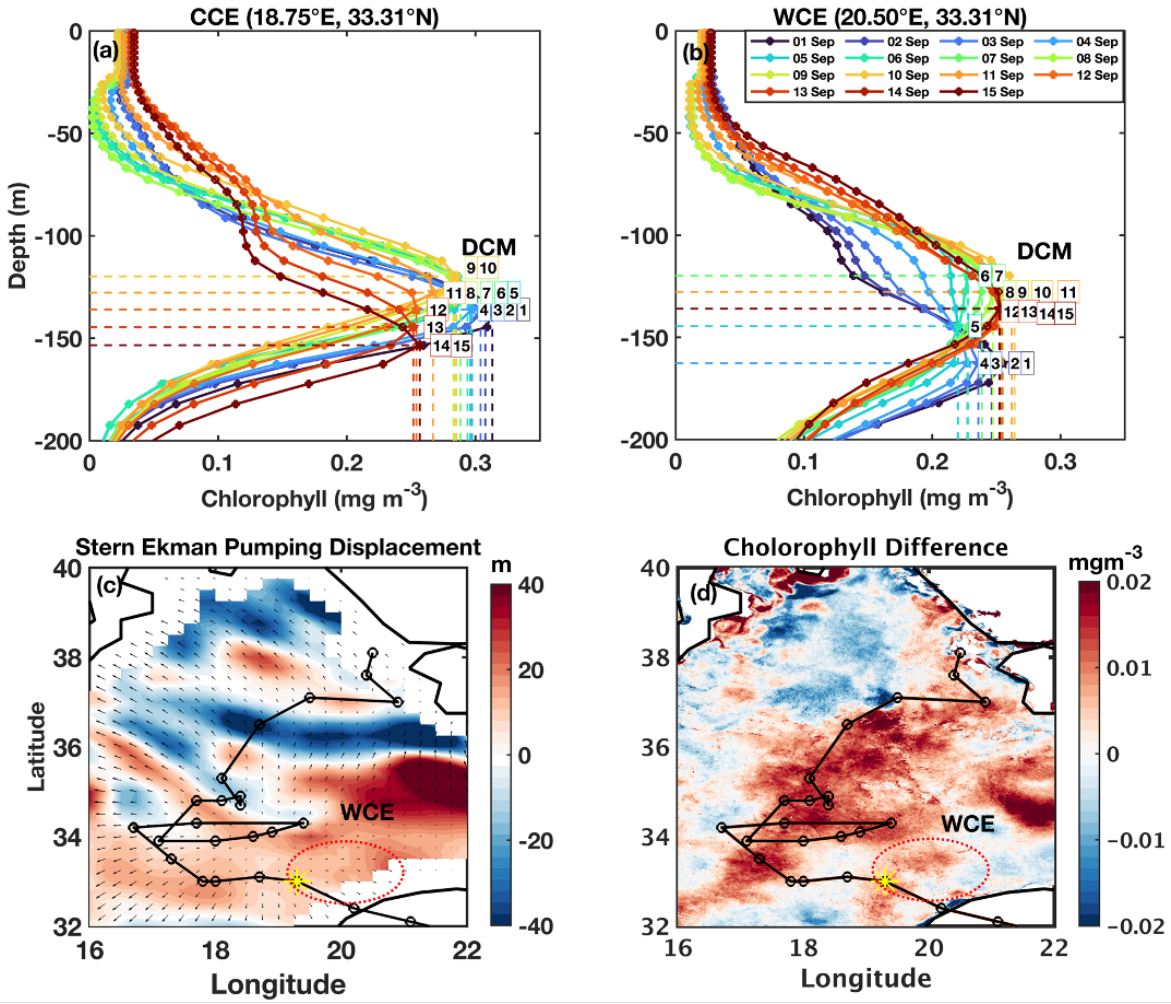

Figure 6: Chorophyll-a profiles from 1 to 15 September 2023 at the cold-core eddy (CCE; a) and warm-core eddy (WCE; b) locations. (c) Cumulative Ekman pumping displacement for 5–9 September 2023, with arrows indicating the transport vector during the cyclone. (d) Satellite chlorophyll-a (2 km spatial resolution) before and after medicane Daniel. The red dotted ellipse indicates the location of the warm-core eddy, and the yellow star denotes the location of maximum cyclone intensity (Max-CI).

5. Conclusions

This case study ~~has provided~~provides comprehensive insights into the intensification and ~~impact~~impacts of ~~the~~ medicane Daniel, which ~~formed in~~developed over the ~~MS~~Mediterranean Sea in September 2023. The findings show the significant role of oceanic and atmospheric variables in cyclone intensification, particularly the presence of WCE and MHW (Figure 7). These oceanic features reduced the negative feedback loop between cyclone intensity and SST, allowing the cyclone to maintain and even increase ~~its~~it's intensity. This study also highlighted

the importance of OHC in providing the energy necessary for cyclone intensification, with approximately 120 KJ/cm² of heat available at the intensification location over the WCE and MHW. Additionally, the convergence of moisture at the locations of the WCE and MHW, combined with the elevated total water column, contributed to the heavy precipitation observed in the coastal areas in Libya.

This study highlights the critical role of high-resolution SWOT data in advancing our understanding of air-sea interaction processes. While CMEMS data, with its coarser spatial resolution, suggests the presence of a weak eddy near the cyclone intensification region, SWOT's finer 2 km resolution reveals a high-intensity WCE precisely aligned with the cyclone's path. This enhanced detection capability provides a more accurate illustration of eddy characteristics and their influence on cyclone dynamics. Furthermore, satellite-derived Chl-a data indicate an enhanced bloom over the WCE location, supported by positive Ekman pumping values. These high values indicate cyclone-induced upward movement of water from deeper layers to the surface, bringing cold, nutrient-rich water to the surface, and boosting ocean productivity.

Subsurface profiles of physical and biogeochemical properties show a notable temperature decrease above the mixed layer depth, particularly over the WCE and MHW regions. The passage of the cyclone triggers vertical mixing, leading to an increase in surface nutrient concentrations. Combined with sufficient sunlight in the euphotic zone, this promotes a surge in surface Chl-a and phytoplankton productivity. Cross-sectional analysis further reinforces these findings: a clear upward shift in isotherms following the cyclone indicates heat loss and active upwelling over the WCE. Concurrently, the ~~chlorophyll~~Chl-a sections display an upward displacement and intensification of ~~chlorophyll~~Chl-a concentrations, confirming the strong biogeochemical response induced by the cyclone's passage over the WCE region.

In conclusion, the study of medicane Daniel emphasizes the need for a deeper understanding of both oceanic and atmospheric factors in predicting and mitigating the impacts of such cyclones in the ~~MR.~~Mediterranean region. The findings suggest that, similar to tropical cyclones in other ocean basins, medicanes are ~~strongly~~significantly influenced by the interplay of oceanic heat content, eddies, and atmospheric dynamics~~, which together determine~~. These factors are responsible for the ~~intensity~~intensification of the cyclone and ~~destructiveness of these storms~~the destruction caused by the medicane.

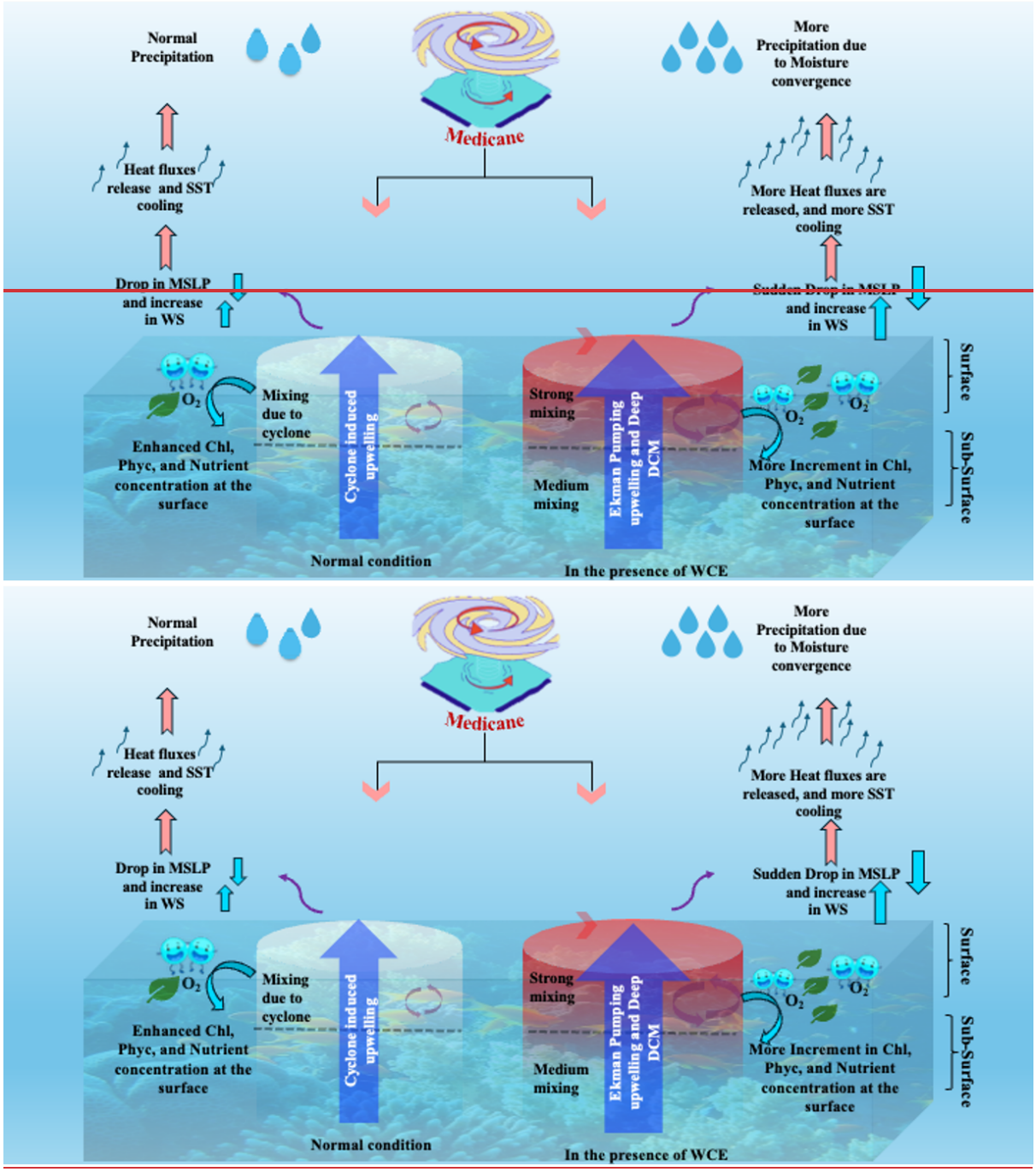

Figure 7: Schematic ~~of~~illustrating the process ~~responsible for the~~associated with cyclone intensification over warm-core eddy and ~~MHW~~marine heatwave, and their impact on ocean biogeochemistry~~.~~

Data Availability:

Data can be Archived from the links below-

~~https://doi.org/10.25423/cmcc/medsea_multiyear_bgc_006_008_medbfm3~~
~~https://doi.org/10.48670/moi-00298~~

https://doi.org/10.25423/cmcc/medsea_multiyear_bgc_006_008_medbfm3
https://doi.org/10.48670/moi-00298
https://zivipotty.hu/tcr.html
https://www.aviso.altimetry.fr/en/data/products/sea-surface-height-products/global/swot-l3-ocean-products.html

Author Contributions:

B.J. contributed to the conceptualization of the study, data curation, formal analysis, and writing of the original draft.

E.S. served as the project investigator, contributed to conceptualization, provided resources and software support, supervised the research, and contributed to ~~writing,~~ review, and editing, as well as funding acquisition.

Competing Interests: The authors declare no conflict of interest.

Acknowledgments: The authors acknowledge the data-providing agencies (i.e., CMEMS, AVISO) for providing data free of cost.

Funding: This research was supported by the Israel Science Foundation (Grant 2228/21).

References

Ali, M. M., Jagadeesh, P. S. V. and Jain, S., 2007. Effects of eddies on Bay of Bengal cyclone intensity, *Eos Trans. AGU*, 88(8), 93–95, doi:10.1029/2007EO080001.

Archer, M., Wang, J., Klein, P. *et al.,* 2025. Wide-swath satellite altimetry unveils global submesoscale ocean dynamics. *Nature* 640, 691–696. https://doi.org/10.1038/s41586-025-08722-8

Avolio, E., Fanelli, C., Pisano, A., & Miglietta, M. M. 2024. Unveiling the relationship between Mediterranean tropical-like cyclones and rising Sea Surface Temperature. *Geophysical Research Letters*, 51, e2024GL109921. https://doi.org/10.1029/2024GL109921

Bender, M. A., Ginis, I., and Kurihara, Y., 1993. Numerical simulations of tropical cyclone-ocean interaction with a high-resolution coupled model, *J. Geophys. Res.*, 98(D12), 23245–23263, doi:10.1029/93JD02370.

Berthon, J.-F., Zibordi, G., 2004. Bio-optical relationships for the northern Adriatic Sea. Int. J. Remote Sens., 25, 1527-1532.

Chen, Y., Pan, G., Mortimer, R., Zhao, H., 2022. Possible Mechanism of Phytoplankton Blooms at the Sea Surface after Tropical Cyclones. *Remote Sensing. 14*, 6207. doi: 10.3390/rs14246207

Cherif, S., Doblas-Miranda, E., Lionello, P., Borrego, C., Giorgi, F., Iglesias, A., et al.,2020. Drivers of change. In *Climate and environmental change in the Mediterranean Basin—current situation and risks for the future* (pp. 59–128). First Mediterranean Assessment Report. Union for the Mediterranean, Plan Bleu, UNEP/MAP.

Chowdhury, R. R., Prasanna Kumar, S., Narvekar, J., & Chakraborty, A., 2020. Back-to-back occurrence of tropical cyclones in the Arabian Sea during October–November 2015: Causes and responses. *Journal of Geophysical Research: Oceans*, 125, e2019JC015836. doi: 10.1029/e2019JC015836

Claud, C., Alhammoud, B., Funatsu, B. M., and Chaboureau, J.-P., 2010. Mediterranean hurricanes: large-scale environment and convective and precipitating areas from satellite microwave observations, Nat. Hazards Earth Syst. Sci., 10, 2199–2213, https://doi.org/10.5194/nhess-10-2199-2010.

Cressman, G. P., 1959. An operational objective analysis scheme. *Monthly Weather Review*, **87**, 367–374. doi: 10.1175/1520-0493(1959)087<0367:aooas>2.0.co;2

Dutta, D., Mani, B. & Dash, M.K., 2019. Dynamic and thermodynamic upper-ocean response to the passage of Bay of Bengal cyclones 'Phailin' and 'Hudhud': a study using a coupled modelling system. *Environ Monit Assess* 191 (Suppl 3), 808.. https://doi.org/10.1007/s10661-019-7704-9.

Emanuel, K.,2005. Genesis and maintenance of "Mediterranean hurricanes." *Advances in Geosciences*, 2, 217–220. https://doi.org/10.5194/adgeo-2-217-2005

Fita, L., Romero, R., Luque, A., Emanuel, K., and Ramis, C., (2007) Analysis of the environments of seven Mediterranean tropical-like storms using an axisymmetric, nonhydrostatic, cloud resolving model, Nat. Hazards Earth Syst. Sci., 7, 41–56, https://doi.org/10.5194/nhess-7-41-2007.

Flaounas, E., Raveh-Rubin, S., Wernli, H., Drobinski, P., and Bastin, S., (2015). The dynamical structure of intense Mediterranean cyclones, Clim. Dynam., 44, 2411–2427, https://doi.org/10.1007/s00382-014-2330-2

Flaounas, E.; Davolio, S.; Raveh-Rubin, S.; Pantillon, F.; Miglietta, M.M.; Gaertner, M.A.; Hatzaki, M.; Homar, V.; Khodayar, S.; Korres, G.; et al., 2022. Mediterranean Cyclones: Current Knowledge and Open Questions on Dynamics, Prediction, Climatology and Impacts. *Weather Clim. Dyn. 3*, 173–208

Flaounas, E., Dafis, S., Davolio, S., Faranda, D., Ferrarin, C., Hartmuth, K., Hochman, A., Koutroulis, A., Khodayar, S., Miglietta, M. M., Pantillon, F., Patlakas, P., Sprenger, M., and Thurnherr, I.: Dynamics, predictability, impacts and climate change considerations of the catastrophic Mediterranean Storm Daniel (2023), Weather Clim. Dynam., 6, 1515–1538, https://doi.org/10.5194/wcd-6-1515-2025, 2025.

Flocas, H. A., 2000. Diagnostics of cyclogenesis over the Aegean sea using potential vorticity inversion, Meteorol. Atmos. Phys., 73, 25–33, https://doi.org/10.1007/s007030050061

González-Alemán, J. J., Pascale, S., Gutierrez-Fernandez, J., Murakami, H., Gaertner, M. A., & Vecchi, G. A. (2019). Potential increase in hazard from Mediterranean hurricane activity with global warming. *Geophysical Research Letters*, 46, 1754–1764. https://doi.org/10.1029/2018GL081253

Hersbach, H., Bell, B., Berrisford, P., Hirahara, S., Horanyi, A., Munoz-Sabatar, J., et al.,2020. The Era5 global reanalysis. *Quarterly Journal of the Royal Meteorological Society*, 146, 1999–2049, doi: 10.1002/qj.3803.

Hérincs, D., 2023. *Tropical Storm Daniel: Mediterranean tropical cyclone report (7–10 September 2023)*. Zivipotty.hu. https://zivipotty.hu/2023_daniel.pdf

Hobday, A. et al., 2016. A hierarchical approach to defining marine heatwaves. *Prog. Oceanogr.* 141, 227–238.

Hobday, A.J., Oliver, E.C.J., Sen Gupta, A., Benthuysen, J.A., Burrows, M.T., Donat, M.G., Holbrook, N.J., Moore, P.J., Thomsen, M.S., Wernberg, T., and Smale, D.A., 2018. Categorizing and naming marine heatwaves. *Oceanography* 31(2):162–173, https://doi.org/10.5670/oceanog.2018.205.

Hochman, A., Scher, S., Quinting, J., Pinto, J. G., & Messori, G.,2021. A new view of heat wave dynamics and predictability over the eastern Mediterranean. *Earth System Dynamics*, 12(1), 133–149. https://doi.org/10.5194/esd-12-133-2021

IPCC., 2021. In V. Masson-Delmotte, P. Zhai, A. Pirani, S. L. Connors, C. Péan, et al. (Eds.), *Climate Change 2021: The Physical Science Basis. Contribution of Working Group I to the Sixth Assessment Report of the Intergovernmental Panel on Climate Change*. Cambridge University Press. https://doi.org/10.1017/9781009157896

Jangir B., Mishra A. K., Strobach, E., 2024. The interplay between medicanes and the Mediterranean Sea in the presence of sea surface temperature anomalies, Atmospheric Research, Volume 310, 107625, ISSN 0169-8095, https://doi.org/10.1016/j.atmosres.2024.107625.

Jangir, B., Mishra, A. K., & Strobach, E.,2023. Effects of mesoscale eddies on the intensity of cyclones in the Mediterranean Sea. *Journal of Geophysical Research: Atmospheres*, 128, e2023JD038607, doi: 10.1029/2023JD038607

Jangir, B., Swain, D., & Ghose, S.,2021. Influence of eddies and tropical cyclone heat potential on intensity changes of tropical cyclones in the North Indian Ocean. *Advances in Space Research*, 68(2), 773–786, doi: 10.1016/j.asr.2020.01.011

Jangir, B., Reale, M., Menna, M., Mishra, A. K., Marellucci, R., Cossarini, G., et al. (2026). The response of the physical and biogeochemical marine environment to the passage of Mediterranean cyclones in the presence of eddies, gyres, and marine heat wave. Journal of Geophysical Research: Oceans, 131, e2025JC023151. https://doi. org/10.1029/2025JC023151

Katsanos, D., Retalis, A., Kalogiros, J., Psiloglou, B. E., Roukounakis, N., & Anagnostou, M.,2024. Performance Evaluation of Satellite Precipitation Products During Extreme Events—The Case of the Medicane Daniel in Thessaly, Greece. *Remote Sensing*, *16*(22), 4216. https://doi.org/10.3390/rs16224216

Khodayar, S., Kushta, J., Catto, J. L., Dafis, S., Davolio, S., Ferrarin, C., et al., 2025. Mediterranean cyclones in a changing climate: A review on their socio-economic impacts. *Reviews of Geophysics*, 63, e2024RG000853. https://doi.org/10.1029/2024RG000853.

Klein, P., and Lapeyre, G., 2009. The Oceanic Vertical Pump Induced by Mesoscale and Submesoscale Turbulence. Annual Review of Marine Science, 1(Volume 1, 2009):351–375, 2009. ISSN 1941-0611. doi:https://doi.org/10.1146/annurev.marine.010908.163704.

Kouroutzoglou, J., Flocas, H. A., Keay, K., Simmonds, I., and Hatzaki, M., 2011. Climatological aspects of explosive cyclones in the Mediterranean, Int. J. Climatol., 31, 1785–1802, https://doi.org/10.1002/joc.2203.

Latha, P. T., Rao, K.H., Nagamani, P.V., Amminedu, E., Choudhury, S.B., Dutt, C.B.S. and Dadhwal, V.K.,2015. Impact of Cyclone PHAILIN on Chlorophyll-a Concentration and Productivity in the Bay of Bengal. *International Journal of Geosciences*, 6, 473-480, doi: 10.4236/ijg.2015.65037.

Law K., 2011. The Impact of Oceanic Heat Content on the Rapid Intensification of Atlantic Hurricanes, Chapter 17. In: Lupo, A., eds. Recent Hurricane Research - Climate, Dynamics, and Societal Impacts. Croatia : InTech: 331-354.

Li, D., Chang, P., Ramachandran, S., Jing, Z., Zhang, Q., Kurian, J., Gopal, A., & Yang, H. (2021). Contribution of the Two Types of Ekman Pumping Induced Eddy Heat Flux to the Total Vertical Eddy Heat Flux. *Geophysical Research Letters*, *48*(9), e2021GL092982. https://doi.org/10.1029/2021GL092982.

Lin, I. I., Goni, G. J., Knaff, J. A., ZForebas, C., Ali, M. M.,2013. Ocean heat content for tropical cyclone intensity forecasting and its impact on storm surge, Nat. Hazards, 66, pp. 1481-1500, 10.1007/s11069-012-0214-5

Liu, Y., Tang, D., Tang, S., Morozov, E., Liang, W., Sui, Y.,2020. A case study of Chlorophyll a response to tropical cyclone Wind Pump considering Kuroshio invasion and air-sea heat exchange. *Science of Total Environment*, 741:140290. doi: 10.1016/j.scitotenv.2020.140290. Epub 2020 Jun 18. PMID: 32603939.

Ma, Z.,2018. Examining the contribution of surface sensible heat flux induced sensible heating to tropical cyclone intensification from the balance dynamics theory. *Dynamics of Atmospheres and Oceans*, 84, 33–45. https://doi.org/10.1016/j.dynatmoce.2018.09.001

MedECC.,2020. Climate and environmental change in the Mediterranean Basin—Current situation and risks for the future. In W. Cramer, J. Guiot, & K. Marini (Eds.), *First Mediterranean assessment report*, Union for the Mediterranean, Plan Bleu (p. 632). UNEP/MAP.

Menna, M., Martellucci, R., Reale, M. *et al.,*2023 A case study of impacts of an extreme weather system on the Mediterranean Sea circulation features: Medicane Apollo (2021). *Scintific Report,* 13, 3870, doi: 10.1038/s41598-023-29942-w.

Miglietta, M.M.,Rotunno, R., 2019. Development Mechanisms for Mediterranean Tropical-like Cyclones (Medicanes). *Q. J. R. Meteorol. Soc. 145*, 1444–1460.

Mishra, A.K., Jangir, B. & Strobach, E., 2024. Influence of mesoscale sea-surface temperature structures on the Mediterranean cyclone Ianos in convection-permitting simulations: Contributions of surface warming and cold wakes. *Quarterly Journal of the Royal Meteorological Society*, 150(765), 5146–5166. https://doi.org/10.1002/qj.4862

Morrow, R., et al.,2019. "Global observations of fine-scale ocean surface topography with the Surface Water and Ocean Topography (SWOT) mission." *Frontiers in Marine Science*, 6, 232. https://doi.org/10.3389/fmars.2019.00232.

Nicolaides, K. A., Michalelides, S. C., and Karacostas, T. (2006). Synoptic and dynamic characteristics of selected deep depressions over Cyprus, Adv. Geosci., 7, 175–180, https://doi.org/10.5194/adgeo-7-175-2006, 2006.

Normand, J.C.L., Heggy, E., 2024. Assessing flash flood erosion following storm Daniel in Libya. *Nat Commun* 15, 6493. https://doi.org/10.1038/s41467-024-49699-8

Oliver, E.C.J., Donat, M.G., Burrows, M.T. *et al., 2018.* Longer and more frequent marine heatwaves over the past century. *Nat Commun* 9, 1324. https://doi.org/10.1038/s41467-018-03732-9

Panegrossi, G., D'Adderio, L. P., Dafis, S., Rysman, J.-F., Casella, D., Dietrich, S., & Sanò, P., 2023. Warm Core and Deep Convection in Medicanes: A Passive Microwave-Based Investigation. *Remote Sensing*, *15*(11), 2838. https://doi.org/10.3390/rs15112838

Pytharoulis, I., Kartsios, S., Tegoulias, I., Feidas, H., Miglietta, M. M., Matsangouras, I., & Karacostas, T.,2018. Sensitivity of a Mediterranean Tropical-Like Cyclone to Physical Parameterizations. *Atmosphere*, *9*(11), 436. https://doi.org/10.3390/atmos9110436

Raveh-Rubin, S. and Flaounas, E., 2017. A dynamical link between deep Atlantic extratropical cyclones and intense Mediterranean cyclones. *Atmospheric Science Letters*, 18: 215-221. https://doi.org/10.1002/asl.745

Reale, M., Cabos, W., Cavicchia, L., Conte, D., Coppola, E., Flaounas, E., et al.,2022. Future projections of Mediterranean cyclone characteristics using the Med-CORDEX ensemble of coupled regional climate system models. *Climate Dynamics*, 58(9–10), 2501–2524. https://doi.org/10.1007/s00382-021-06018-x

Reynolds, R. W., Smith, T. M., Liu, C., Chelton, D. B., Casey, K. S., and Schlax, M. G., 2007. Daily High-Resolution-Blended Analyses for Sea Surface Temperature. *J. Climate*, 20, 5473–5496, https://doi.org/10.1175/2007JCLI1824.1.

Scardino, G., Kushabaha, A., Miglietta, M. M., Bonaldo, D., and Scicchitano, G.: When storms stir the Mediterranean depths: chlorophyll *a* response to Mediterranean cyclones, Ocean Sci., 21, 2849–2872, https://doi.org/10.5194/os-21-2849-2025, 2025.

Scardino, G., Miglietta, M.M., Kushabaha, A. *et al.,2024.* Fingerprinting Mediterranean hurricanes using pre-event thermal drops in seawater temperature. *Sci Rep* 14, 8014. https://doi.org/10.1038/s41598-024-58335-w

Shang, X.-D., Zhu, H.-B., Chen, G.-Y., Xu, C., & Yang, Q.,2015. Research on cold core eddy change and phytoplankton bloom induced by typhoons: Case studies in the South China Sea. *Advances in Meteorology*, 1–19.doi: 10.1155/2015/340432.

Shang, X.-D., Zhu, H.-B., Chen, G.-Y., Xu, C., & Yang, Q.,2015. Research on cold core eddy change and phytoplankton bloom induced by typhoons: Case studies in the South China Sea. *Advances in Meteorology*, 1–19.doi: 10.1155/2015/340432.

Sharma, V., & Ali, M. M.,2014. Importance of ocean heat content for cyclone studies. *Journal of Climatology & Weather Forecasting, 2*(1), 1–6. https://www.longdom.org/open-access/importance-of-ocean-heat-content-for-cyclone-studies-9577.html

Strobach, E., Mishra, A.K., Jangir, B. *et al., 2024.* Intensification of a rain system imparted by Mediterranean mesoscale eddies. *Sci Rep* 14, 26810. https://doi.org/10.1038/s41598-024-76767-2

Stern, M., 1965, Interaction of a uniform wind stress with a geostrophic vortex, *Deep Sea Res. Oceanogr. Abstr.*, 12(3), 355–367.

Sun, M., Tian, F., Liu, Y., & Chen, G., 2017. An Improved Automatic Algorithm for Global Eddy Tracking Using Satellite Altimeter Data. *Remote Sensing*, *9*(3), 206. https://doi.org/10.3390/rs9030206

Trigo, I. F., Bigg, G. R., and Davies, T. D., 2002. Climatology of cyclogenesis mechanisms in the Mediterranean, Mon. Weather Rev., 130, 549–569.

Vidya, P. J., Balaji, M., Mani Murali, R., 2021. Cyclone Hudhud-eddy induced phytoplankton bloom in the northern Bay of Bengal using a coupled model, Progress in Oceanography, Volume 197, 102631, ISSN 0079-6611, https://doi.org/10.1016/j.pocean.2021.102631.

Volpe, G., Buongiorno Nardelli, B., Colella, S., Pisano, A. and Santoleri, R.,2018. An Operational Interpolated Ocean Colour Product in the Mediterranean Sea, in New Frontiers in Operational Oceanography, edited by E. P. Chassignet, A. Pascual, J. Tintorè, and J. Verron, pp. 227–244.

Volpe, G., Colella, S., Brando, V. E., Forneris, V., Padula, F. L., Cicco, A. D., & Santoleri, R.,2019. Mediterranean Ocean Colour Level 3 operational multi-sensor processing. Ocean Science, 15(1), 127-146.

Wada, A., & Usui, N.,2007. Impact of tropical cyclone heat potential on tropical cyclone intensity in the western North Pacific Ocean. *Journal of Oceanography, 63*(3), 505–516. https://doi.org/10.1007/s10872-007-0039-0

Wada, A., Usui, N., 2007. Importance of tropical cyclone heat potential for tropical cyclone intensity and intensification in the Western North Pacific. *J Oceanogr* 63, 427–447. https://doi.org/10.1007/s10872-007-0039-0

Tranchant, Y. T., Legresy, B., Foppert, A., et al., 2025. SWOT reveals fine-scale balanced motions and dispersion properties in the Antarctic Circumpolar Current. *ESS Open Archive* . 10.22541/essoar.173655552.25945463/v1

Zhang, Z., & Qiu, B.,2020. Surface Chlorophyll Enhancement in Mesoscale Eddies by Submesoscale Spiral Bands. *Geophysical Research Letters*, 47, e2020GL088820. https://doi.org/10.1029/2020GL088820

Zhao et al., 2019. A MATLAB toolbox to detect and analyze marine heatwaves. Journal of Open Source Software, 4(33), 1124, https://doi.org/10.21105/joss.01124

Zittis, G., Almazroui, M., Alpert, P., Ciais, P., Cramer, W., Dahdal, Y., et al.,2022. Climate change and weather extremes in the Eastern Mediterranean and Middle East. *Reviews of Geophysics*, 60(3), e2021RG000762. https://doi.org/10.1029/2021RG000762.